ISME

# Nonlinear Analysis of Integrated Kinetics and Heat Transfer Models of Slow Pyrolysis of Biomass Particles using Differential Transformation Method

**M. G. Sobamowo***
Assistant Professor

**S. J. Ojolo**†
Associate Professor

**C. A. Osheku**‡
Associate Professor

*The inherent nonlinearities in the kinetics and heat transfer models of biomass pyrolysis have led to the applications of various numerical methods in solving the nonlinear problems. However, in order to have physical insights into the phenomena and to show the direct relationships between the parameters of the models, analytical solutions are required. In this work, approximate analytical solutions for the nonlinear integrated kinetics and heat transfer of pyrolysis of biomass particle under isothermal and non-isothermal heating conditions are presented using differential transformation method. Also, the results of the analytical solutions are compared with the numerical and experimental results in literature. Good agreements are established between the present results and the past works. Thereafter, parametric studies are carried out on the effects of heating conditions, heating rates, thermo-geometric parameters, boundary conditions, particles shape and size on the pyrolysis kinetics and thermal decomposition of biomass particles. It is therefore expected that this study will enhance the understanding of the pyrolysis by giving physical insights into the various factors and the parameters affecting the thermochemical process.*

*Keywords:* Biomass particle; Pyrolysis kinetics; Isothermal temperature; Non- isothermal heating rates; Differential transformation method.

## 1 Introduction

The importance and the centrality of pyrolysis in thermochemical biomass conversion of biomass have increased the research interests in the studies of biomass gasification. In the thermochemical processing of biomass, the overall process of pyrolysis entails sequence of reactions which are very complex. This is because, it involves endothermic and exothermic processes which their thermodynamics and kinetics are poorly understood [1].

* Assistant Professor, Department of Mechanical Engineering, University of Lagos, Akoka, Lagos, Nigeria, mikegbeminiyi@gmail.com

† Associate Professor, Department of Mechanical Engineering, University of Lagos, Akoka, Lagos, Nigeria, ojolosunday@yahoo.com

‡ Associate Professor, Centre for Space Transport and Propulsion, National Space Research and Development Agency, Federal Ministry of Science and Technology, FCT, Abuja, Nigeria, gsobamowo@unilag.edu.ng

Under such complex phenomena, it is impossible to formulate a complete mathematical model of pyrolysis that will be mathematically tractable. Additionally, the complications involved in the numerical solutions of the sophisticated models make them unsuitable for design and prediction purposes [1]. However, as a compromise between mathematical tractability and accuracy of description, simplified models are employed under certain defined conditions to predict the pyrolytic conversion process of biomass particle. Indisputably, the need for the simple rationally-based models of pyrolysis as a basis for reactor design has been identified in the survey of low temperature (< 600ºC) pyrolytic conversion of biomass. The developed simple and economic models are still able to aggregate the more important aspects of the sequence of events as a solid sample is pyrolyzed. In an early work on the thermochemical models, assuming a first order single step reaction, Bamford [2] combined the heat conduction equations in a pyrolysizing solid fuel with heat generation. Based on the Bamford's model, further studies by various researchers [3, 4, and 5] have been presented.

In some subsequent works Matsumoto et al. [6], Roberts [7] and Kung [8], effects of internal convection and variable transport properties on the pyrolysis process incorporated in the thermal models. Kung [8] investigated the effect of char formation on the pyrolysis process while Matsumoto et al [6] analyzed the rate of char removal during the process. In these studies, the physical and thermal properties of the biomass particles have been assumed invariants. However, in reality, the thermal properties of the biomass during the pyrolysis process vary with temperature. Consequently, different studies on pyrolysis analysis using the temperature-dependent properties were presented by Matsumoto et al [6], Kung [8], Maa and Baille [9], Kansa *et al*. [10], Chan et al, [11]. In some other studies, the limitations of the first-order single step kinetic models for the prediction of the pyrolysis process have been pointed out [8-12]. Therefore, in order to increase the accuracy of the prediction of kinetic models, Kung [8], Chan *et al*. [11] and Koufopanos *et al*. [12] presented multi-step reaction schemes.

Also, Lee et al. [13] modeled the heat of reaction of pyrolysis while the effect of anisotropy of the pyrolysing medium has been considered by Kansa *et al*. [10]. In another work, Maa and Baille [9] proposed an 'unreacted shrinking core model' for high temperatures pyrolysis process while Miyanamie [14] studied the effects of heat of reaction and Lewis number on the pyrolysis of solid particle. For the motion of the gases within the solid, a momentum equation was included by Kansa *et al.* [10]. In the same year, Fan *et al.* [15] developed a 'volume reaction' model taking into account simultaneous heat and mass transfer in the particle.

In an earlier study, Pyle and Zaror [1] experimentally investigated pyrolysis of biomass. Few years later, Simmons [16] analyzed a simplified heat transfer model with an assumed first order reaction for the estimation of an upper bound for biomass particle size in conducting experimental pyrolysis kinetic. In the same year, Villermaux *et al.* [17] presented a Volatilization Thermal Penetration model (VTP) for any kind of solid reaction where volatilization is controlled by heat conduction from the outer surface. On the modeling of pyrolysis of biomass particle, particularly on the studies of the kinetic, thermal and heat transfer effects, Koufopanos *et al*. [12] assumed the pyrolysis process to be primary and secondary kinetic reactions. Using the model of Koufopanos et al., Di Blasi [18] analysed the effects of convection and secondary reactions within porous solid fuels undergoing pyrolysis. Melaaen and Gronli [19] presented models on moist wood drying and pyrolysis. Jalan and Srivastava [20] explored kinetic and heat transfer effects on the pyrolysis of a single biomass cylindrical pellet. In a further study on kinetic of biomass pyrolysis, Ravi [21] proposed a semi-empirical model for pyrolysis of sawdust in an annular packed bed using pseudo-first order reaction for the chemical reaction of the pyrolysis. Meanwhile, Babu and Chaurasia [22] considered time-dependent density and temperature-dependent specific heat capacity of biomass to investigate the dominant design variables in pyrolysis of biomass particles of different geometries in a thermally thick regime.

In the recent time, Sheth and Babu [23], presented kinetic model for biomass pyrolysis and concluded that pyrolysis in wood is typically initiated at 200°C and lasts till 450-500°C, depending on the species of wood. Three years later, Yang *et al.* [24] presented that the major stage of biomass pyrolysis occurs between 250-450ºC. In another study, Mandl *et al*. [25] pointed out that the pyrolysis of softwood pellets takes place at around 425K and char particles and volatiles are formed while Weerachanchai *et al*. [26] submitted that the major decomposition of all biomasses occurred in the range of 250-400ºC. In their study on poplar wood, Slopiecka *et al*. [27] concluded that the decomposition of hemicelluloses and cellulose take place in active pyrolysis in the temperature from 473-653K and 523-623K, respectively. The authors added that Lignin decomposes in both stages: active and passive pyrolysis in the range from 453-1173K without characteristics peaks. In recent times, further investigations into the mechanisms of biomass kinetics are presented [28-51].

In most of the previous works, the present nonlinearity of the improved thermal models necessitated the use of numerical methods to provide solutions to the nonlinear thermal models of biomass pyrolysis [1-26]. Moreover, the analytical solutions (exact/closed form solutions) of the developed pyrolysis models of the study under investigation have been stated to be 'involved' [51]. However, the classical way of finding analytical solution is obviously still very important since it serves as an accurate benchmark for numerical solutions.

Additionally, analytical solutions are essential for the developments and verifications of efficient applied numerical simulation tools. They show the direct relationship between the models parameters. When such analytical solutions are available, they provide good insights into the significance of various system parameters affecting the phenomena as they give continuous physical insights than pure numerical or computation methods. Also, they are convenient for parametric studies, accounting for the physics of the problem and as they more appealing than the numerical solutions. In the bids of establishing analytical solutions for the pyrolysis process However, Ojolo et al. [52] and Sobamowo et al. [53-55] developed analytical solutions for kinetic and heat transfer models in slow pyrolysis of biomass particles.

In another study, Bidabadi *et al.* [56] submitted an analytical model for flame propagation through moist lycopodium particles while Dizaji and Bidabadi [57] presented analytical study on kinetics of different processes in pyrolysis of lycopodium dust. Most of the studies on the development of analytical solutions are based on the assumptions of constant thermal properties. Such studies are limited to very low temperature pyrolysis process where the thermophysical properties are approximately constant.

To the best of authors' knowledge, the development of analytical solutions of pyrolysis kinetics and thermal models of different shapes of biomass particles using differential transformation method has not been carried out in literature. Also, the analytical study of the effects of biomass particle shapes on the thermal decomposition of biomass particles and the effects of different outer boundary and heating conditions on the pyrolysis of biomass have not been really investigated in the past work. Moreover, the quantification of the heating rates for different pyrolysis technologies, which is of utmost importance in the biomass conversion processes, has not been studied in detail.

Therefore, in this study differential transformation method is used to present analytical solutions for integrated nonlinear kinetics and heat transfer models for the pyrolysis of biomass particle of different regular shapes under different outer boundary and heating conditions. Simulations are carried out to study the effects of isothermal, non-isothermal heating conditions, particle size, particle shapes, and boundary conditions on the pyrolysis kinetics and thermal decomposition of biomass particles.

## 2 Mechanism of biomass particle pyrolysis kinetics and heat transfer

When heat is transferred by conduction, radiation and/or convection from the hot gases surrounding the biomass to the surface of the biomass particle and then by conduction to the interior of the particle Fig. (1), the temperature inside the particles increases as the heat penetrates more into the solid causing drying off the moisture from the biomass. The rate of such drying process depends on the temperature, velocity, and moisture content of the drying gas as well as the external surface area of the feed material, the internal diffusivity of moisture and the nature of bonding of moisture to that material, and the radiative heat transfer. As the temperature increases, the biomass particle decomposes into charcoal, tar and gaseous products as shown in Fig. (2). The amounts of each of these products vary depending on the zone temperature, rate of heating, structure, and composition and size of catalysts.

### *a. Model development for the biomass pyrolysis process*

Fig. (3) shows the kinetic scheme that describes the process of pyrolysis (primary and secondary). The pyrolysis process involves thermal decomposition of biomass into gases, tar (liquid product of biomass pyrolysis, known as bio-oil or pyrolysis oil) and char, and the tar further decompose into char and gases.

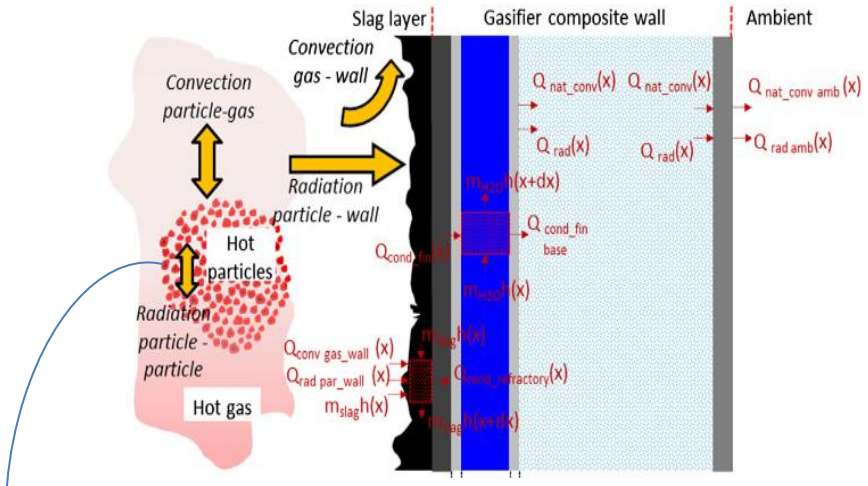


**Figure 1** Heat transfer process during the pyrolysis of biomass particle in biomass gasifier

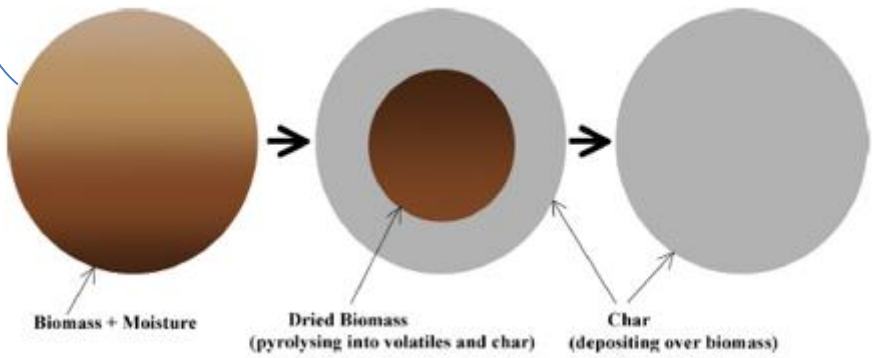


**Figure 2** Schematic diagram shown the decomposition progress of biomass pyrolysis

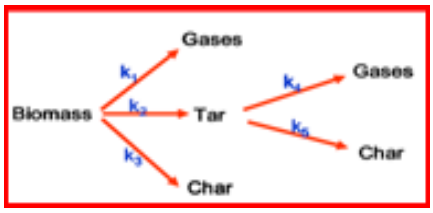


**Figure 3** Two-stage parallel reaction model of biomass pyrolysis

The two-stage parallel reaction model of biomass pyrolysis has previously been adopted by other researchers [10, 13, 17, 18, 19, 21, and 61]. According to the two-stage parallel reaction model, the biomass undergoes thermal degradation according to primary reactions *($k_1$; $k_2$; $k_3$)* giving gas, tar and char as products. Tar may undergo secondary reactions *($k_4$, $k_5$)*.
This model shows to be the most classical models for wood pyrolysis [65].

The kinetic of the pyrolysis process are given as

$$\frac{\partial C_B}{\partial t} = -(k_1 + k_2 + k_3)C_B \tag{1a}$$

$$\frac{\partial C_T}{\partial t} = k_2 C_B - \varepsilon(k_4 + k_5)C_T \tag{1b}$$

$$\frac{\partial C_C}{\partial t} = k_3 C_B + \varepsilon k_5 C_T \tag{1c}$$

$$\frac{\partial C_G}{\partial t} = k_1 C_B + \varepsilon k_4 C_T \tag{1d}$$

where

$$k_i = A_i \exp\left[\left(\frac{-E_i}{RT}\right)\right] \qquad i = 1-5$$

The initial conditions for the kinetic equations are;

$$t = 0, C_B = C_{B0}, C_C = C_G = C_T = 0 \tag{2}$$

For the Isothermal condition, $T=T_o$

$$k_i = A_i \exp\left[\left(\frac{-E_i}{RT_o}\right)\right] \qquad i = 1-5 \tag{3}$$

Srivastava [23] assumed that in the thermo-gravimetric analysis, the temperature and time have a linear relationship (non-isothermal heating condition). This therefore led to the appropriate representation to describe the Srivastava's assumption as;

$$T = T_o + \beta t \tag{4}$$

Where $T_o$ is the initial temperature in *K*, $\beta$ is the heating rate in *K/s* and t is the time in s. Which makes

$$k_i = A_i \exp\left[\left(\frac{-E_i}{R(T_o+\beta t)}\right)\right] \qquad i=1-5 \tag{5}$$

The above kinetic models are non-dimensionalized using the following dimensionless parameters;

$$\overline{C}_B = \frac{C_B}{C_{Bo}} \quad \overline{C}_{G1} = \frac{C_{G1}}{C_{Bo}} \quad \overline{C}_{C1} = \frac{C_{C1}}{C_{Bo}} \quad \overline{C}_{G2} = \frac{C_{G2}}{C_{Bo}} \quad \overline{C}_{C2} = \frac{C_{C2}}{C_{Bo}} \quad C_{C2} = \frac{\overline{C}_{C2}}{C_{Bo}} \tag{6}$$

However, for the sake of cleanliness, the bars on the equations are removed in the solutions and the non-dimensionless forms of Eqs. (1a-1d) are exactly the same as the equations. In order to avoid writing seemingly similar equations, the non-dimensionless forms of Eqs. (1a-1d) are not written out in this work.

### *2.2. Heat transfer model of pyrolysis of biomass particle*

Following the assumptions as given by Pyle and Zaror [1], the heat conduction equation for the biomass particles is given by Eq.(6)

$$\frac{\partial\left(\rho c_p T\right)}{\partial t} = \frac{1}{\hbar^n}\frac{\partial}{\partial \hbar}\left(K\hbar^n \frac{\partial T}{\partial \hbar}\right) + Q_{reaction} \tag{7}$$

where

*$\hbar$= x, n=0 for rectangular shaped particle*
*$\hbar$= r, n=1 for cylindrical shaped particle*
*$\hbar$= r, n=2 for spherical shaped particle*

The temperature-dependent thermal properties are defined as

$$c_p = c_{p,0}\left(1+\psi T\right), \quad K = K_0\left(1+\upsilon T\right) \tag{8}$$

For wood, $c_{p,o} = 1112, \quad \psi = 0.004361511, \quad K_o = 0.13, \quad \upsilon = 0.002307692$

#### *2.2.1 Case 1: Particle surface temperature with convective and radiative heat transfer*

The first case considered in this work is when the outer boundary of the biomass particle is subjected to convective and radiative heat transfer. For this case, the initial and the boundary conditions are;
The initial and the boundary conditions are;

$$\begin{aligned} &t = 0, \quad T = T_o \\ &t > 0, \quad \left(\frac{\partial T}{\partial \hbar}\right)_{\hbar=0} = 0 \\ &t > 0, \quad -k\left(\frac{\partial T}{\partial \hbar}\right)_{\hbar=H} = h\left(T_f - T\right) + \sigma \in \left(T_f^4 - T^4\right) \end{aligned} \tag{9}$$

*2.2.2 Case 2: Particle surface temperature with high external heating fluxes*

A second case of the heat transfer in the biomass particle during the pyrolysis process is considered. In this case, it is assumed in the outer boundary condition that the surface temperature of the slab is specified with high external heating fluxes available using fluidized beds, radiation, or other devices [16].
Under such scenario, the initial and the boundary conditions are;

The initial and the boundary conditions are;

$$\begin{aligned} t = 0, \quad & T = T_o \\ t > 0, \quad & \left(\frac{\partial T}{\partial \hbar}\right)_{\hbar=0} = 0 \\ t > 0, \quad & T_{\hbar=H} = T_0 \end{aligned} \tag{10}$$

On substituting Eq. (8) into Eq. (7), after expansion, one develops the thermal model for rectangular shaped biomass particle as

$$\rho c_{p,0}\left(1+2\psi T\right)\frac{\partial T}{\partial t} = K_0\left(\left(1+\upsilon T\right)\frac{\partial^2 T}{\partial x^2} + \upsilon\left(\frac{\partial T}{\partial x}\right)^2\right) + Q_{reaction} \tag{11}$$

When the outer boundary of the biomass particle is subjected to convective and radiative heat transfer, the initial and the boundary conditions are;

$$\begin{aligned} t = 0, \quad & T = T_o \\ t > 0, \quad & \left(\frac{\partial T}{\partial x}\right)_{x=0} = 0 \\ t > 0, \quad & -k\left(\frac{\partial T}{\partial x}\right)_{x=L} = h\left(T_f - T\right) + \sigma \in \left(T_f^4 - T^4\right) \end{aligned} \tag{12}$$

Where

$$h = 0.322\left(\frac{K}{L}\right)Pr^{1/3}Re^{0.5} \tag{12}$$

When the surface temperature of the slab is specified with high external heating fluxes, the initial and the boundary conditions are;

$$\begin{aligned} t = 0, \quad & T = T_o \\ t > 0, \quad & \left(\frac{\partial T}{\partial x}\right)_{x=0} = 0 \\ t > 0, \quad & T_{x=L} = T_0 \end{aligned} \tag{13}$$

It should be noted that the 'Q' (the pyrolysis enthalpy source term due to conversion) in Equ. (7) is found according to the two-step reaction mechanism as

$$Q_{reaction} = \sum_{i=1}^{3} k_i C_B \Delta h_i + \sum_{4}^{5} k_i C_T \Delta h_i \tag{14}$$

Substituting Eq. (14) into Eq. (11), we have

$$\rho c_{p,0}\left(1+2\psi T\right)\frac{\partial T}{\partial t}=K_0\left(\left(1+\upsilon T\right)\frac{\partial^2 T}{\partial x^2}+\upsilon\left(\frac{\partial T}{\partial x}\right)^2\right)+\sum_{i=1}^{3}k_i C_B\Delta h_i+\sum_{4}^{5}k_i C_T\Delta h_i \qquad (15)$$

The reaction rate coefficient is "exponential" with temperature which renders the Eq. (15) highly nonlinear. The Taylor's series expansion of the nonlinear form upto the fifth term is given as:

$$k_i=Ae^{-\frac{E_i}{R_gT_o}}\left(\begin{array}{l}1+\frac{E}{R_gT_o^2}(T-T_o)+\frac{E}{2R_gT_o^3}\left(\frac{E}{R_gT_o}-2\right)(T-T_o)^2\\+\frac{E}{6R_gT_o^4}\left(\left(\frac{E}{R_gT_o}\right)^2-\frac{6E}{R_gT_o}+6\right)(T-T_o)^3\\+\frac{E}{24R_gT_o^5}\left(\left(\frac{E}{R_gT_o}\right)^3-12\left(\frac{E}{R_gT_o}\right)^2-\frac{36E}{R_gT_o}-24\right)(T-T_o)^4\end{array}\right) \qquad (16)$$

Substituting Eq. (16) into Eq. (14), we arrived at

$$\begin{aligned}Q_{reaction}=&\sum_{i=1}^{3}A_ie^{-\frac{E_i}{R_gT_o}}\left(\begin{array}{l}1+\frac{E_i}{R_gT_o^2}(T-T_o)+\frac{E_i}{2R_gT_o^3}\left(\frac{E_i}{R_gT_o}-2\right)(T-T_o)^2\\+\frac{E_i}{6R_gT_o^4}\left(\left(\frac{E_i}{R_gT_o}\right)^2-\frac{6E_i}{R_gT_o}+6\right)(T-T_o)^3\\+\frac{E_i}{24R_gT_o^5}\left(\left(\frac{E_i}{R_gT_o}\right)^3-12\left(\frac{E_i}{R_gT_o}\right)^2-\frac{36E_i}{R_gT_o}-24\right)(T-T_o)^4\end{array}\right)C_B\Delta h_i\\&+\sum_{i=4}^{5}A_ie^{-\frac{E_i}{R_gT_o}}\left(\begin{array}{l}1+\frac{E_i}{R_gT_o^2}(T-T_o)+\frac{E_i}{2R_gT_o^3}\left(\frac{E_i}{R_gT_o}-2\right)(T-T_o)^2\\+\frac{E_i}{6R_gT_o^4}\left(\left(\frac{E_i}{R_gT_o}\right)^2-\frac{6E_i}{R_gT_o}+6\right)(T-T_o)^3\\+\frac{E_i}{24R_gT_o^5}\left(\left(\frac{E_i}{R_gT_o}\right)^3-12\left(\frac{E_i}{R_gT_o}\right)^2-\frac{36E_i}{R_gT_o}-24\right)(T-T_o)^4\end{array}\right)C_T\Delta h_i\end{aligned} \qquad (17)$$

Substituting Eq. (17) into Eq. (15), gives

$$\rho c_{p,0}\left(1+2\psi T\right)\frac{\partial T}{\partial t}=K_0\left(\left(1+\upsilon T\right)\frac{\partial^2 T}{\partial x^2}+\upsilon\left(\frac{\partial T}{\partial x}\right)^2\right)$$

$$+\left\{\sum_{i=1}^{3}\left\{A_i e^{-\frac{E_i}{R_g T_o}}\left(\begin{array}{l}1+\frac{E_i}{R_g T_o^2}(T-T_o)+\frac{E_i}{2R_g T_o^3}\left(\frac{E_i}{R_g T_o}-2\right)(T-T_o)^2\\+\frac{E_i}{6R_g T_o^4}\left(\left(\frac{E_i}{R_g T_o}\right)^2-\frac{6E_i}{R_g T_o}+6\right)(T-T_o)^3\\+\frac{E_i}{24R_g T_o^5}\left(\left(\frac{E_i}{R_g T_o}\right)^3-12\left(\frac{E_i}{R_g T_o}\right)^2-\frac{36E_i}{R_g T_o}-24\right)(T-T_o)^4\end{array}\right)C_B\Delta h_i\right\}\right.$$

$$\left.+\sum_{i=4}^{5}\left\{A_i e^{-\frac{E_i}{R_g T_o}}\left(\begin{array}{l}1+\frac{E_i}{R_g T_o^2}(T-T_o)+\frac{E_i}{2R_g T_o^3}\left(\frac{E_i}{R_g T_o}-2\right)(T-T_o)^2\\+\frac{E_i}{6R_g T_o^4}\left(\left(\frac{E_i}{R_g T_o}\right)^2-\frac{6E_i}{R_g T_o}+6\right)(T-T_o)^3\\+\frac{E_i}{24R_g T_o^5}\left(\left(\frac{E_i}{R_g T_o}\right)^3-12\left(\frac{E_i}{R_g T_o}\right)^2-\frac{36E_i}{R_g T_o}-24\right)(T-T_o)^4\end{array}\right)C_T\Delta h_i\right\}\right\} \quad (18)$$

Using the following dimensionless parameter to transform the equations, the initial and the boundary conditions to non-dimensionless forms;

$$\theta=\frac{T-T_0}{T_f-T_0},\ \varphi=\frac{T_0}{T_f-T_0},\ \tau=\frac{K_o t}{\rho c_{p,o}L^2},\ \alpha=\frac{QAL^2 e^{-E/RT_o}}{K(T_f-T_0)},\ \ \lambda=2\psi\left(T_f-T_0\right),$$

$$\zeta=\upsilon\left(T_f-T_0\right),\ X=\frac{x}{L},\ \beta_o=\sum_{i=1}^{3}A_i e^{-\frac{E_i}{R_g T_o}}\Delta h_i,\ \beta_1=\sum_{i=1}^{3}A_i e^{-\frac{E_i}{R_g T_o}}\left(\frac{E_i(T_f-T_o)}{RT_o^2}\right)\Delta h_i,$$

$$\beta_2=\sum_{i=1}^{3}A_i e^{-\frac{E_i}{R_g T_o}}\left(\frac{2E_i}{RT_o^3}\right)\left(\frac{E_i}{2RT_o}-1\right)(T_f-T_o)^2\Delta h_i$$

$$\beta_3=\sum_{i=1}^{3}A_i e^{-\frac{E_i}{R_g T_o}}\left(\left(\frac{E}{R_g T_o}\right)^2-\frac{6E}{R_g T_o}+6\right)\left(\frac{E_i}{6R_g T_o^4}\right)(T_f-T_o)^3\Delta h_i,$$

$$\beta_4=\sum_{i=1}^{3}A_i e^{-\frac{E_i}{R_g T_o}}\left(\frac{E_i}{24R_g T_o^5}\right)\left(\left(\frac{E_i}{R_g T_o}\right)^3-12\left(\frac{E_i}{R_g T_o}\right)^2-\frac{36E_i}{R_g T_o}-24\right)(T_f-T_o)^4\Delta h_i,$$

$$\gamma_1=\sum_{i=4}^{5}A_i e^{-\frac{E_i}{R_g T_o}}\left(\frac{E_i(T_f-T_o)}{RT_o^2}\right)\Delta h_i,\ \gamma_2=\frac{2E}{RT_o^3}\sum_{i=4}^{5}A_i e^{-\frac{E_i}{R_g T_o}}\left(\frac{E}{2RT_o}-1\right)(T_f-T_o)^2\Delta h_i$$

$$\gamma_o=\sum_{i=4}^{5}A_i e^{-\frac{E_i}{R_g T_o}}\Delta h_i,\ \gamma_3=\frac{E}{6R_g T_o^4}\sum_{i=4}^{5}A_i e^{-\frac{E_i}{R_g T_o}}\left(\left(\frac{E}{R_g T_o}\right)^2-\frac{6E}{R_g T_o}+6\right)(T_f-T_o)^3\Delta h_i$$

$$\gamma_4=\sum_{i=4}^{5}A_i e^{-\frac{E_i}{R_g T_o}}\left(\frac{E_i}{24R_g T_o^5}\right)\left(\left(\frac{E_i}{R_g T_o}\right)^3-12\left(\frac{E_i}{R_g T_o}\right)^2-\frac{36E_i}{R_g T_o}-24\right)(T_f-T_o)^4\Delta h_i$$

The heat transfer model is developed in dimensionless form is gives as

$$\left(1+\lambda\left(\theta\left(X,\tau\right)+\varphi\right)\right)\frac{\partial\theta\left(X,\tau\right)}{\partial\tau}=\left(1+\zeta\left(\theta\left(X,\tau\right)+\varphi\right)\right)\frac{\partial^2\theta\left(X,\tau\right)}{\partial X^2}+\zeta\left(\frac{\partial\theta\left(X,\tau\right)}{\partial X}\right)^2$$
$$-\alpha\left\{\begin{bmatrix}\beta_0+\beta_1\theta\left(X,\tau\right)+\beta_2\theta^2\left(X,\tau\right)\\+\beta_3\theta^3\left(X,\tau\right)+\beta_4\theta^4\left(X,\tau\right)\end{bmatrix}C_B\left(\tau\right)\right.$$
$$\left.+\begin{bmatrix}\gamma_0+\gamma_1\theta\left(X,\tau\right)+\gamma_2\theta^2\left(X,\tau\right)\\+\gamma_3\theta^3\left(X,\tau\right)+\gamma_4\theta^4\left(X,\tau\right)\end{bmatrix}C_T\left(\tau\right)\right\} \tag{19}$$

And the dimensionless initial and boundary conditions are

$$\begin{aligned}&\tau=0,\quad \theta\left(X,0\right)=0\\&\tau>0,\quad X=0,\quad \frac{\partial\theta}{\partial X}=0\\&\tau>0,\quad X=1,\quad \frac{\partial\theta}{\partial X}=Bi_m\theta+Bi_r\left[\left(\theta+\varphi\right)^4-\varphi^4\right]\end{aligned} \tag{20}$$

Similarly, the heat transfer model for the cylindrical-shaped particle is developed in dimensionless form as

$$\left(1+\lambda\left(\theta\left(R,\tau\right)+\varphi\right)\right)\frac{\partial\theta\left(R,\tau\right)}{\partial\tau}=\left(1+\zeta\left(\theta\left(R,\tau\right)+\varphi\right)\right)\frac{\partial^2\theta\left(R,\tau\right)}{\partial R^2}$$
$$+\zeta\left(\frac{\partial\theta\left(R,\tau\right)}{\partial R}\right)^2+\frac{\left(1+\zeta\left(\theta\left(R,\tau\right)+\varphi\right)\right)}{R}\frac{\partial\theta\left(R,\tau\right)}{\partial R}-\alpha\left\{\begin{bmatrix}\beta_0+\beta_1\theta\left(R,\tau\right)+\beta_2\theta^2\left(R,\tau\right)\\+\beta_3\theta^3\left(R,\tau\right)+\beta_4\theta^4\left(R,\tau\right)\end{bmatrix}C_B\left(\tau\right)\right.$$
$$\left.+\begin{bmatrix}\gamma_0+\gamma_1\theta\left(R,\tau\right)+\gamma_2\theta^2\left(R,\tau\right)\\+\gamma_3\theta^3\left(R,\tau\right)+\gamma_4\theta^4\left(R,\tau\right)\end{bmatrix}C_T\left(\tau\right)\right\} \tag{21}$$

And the initial and boundary conditions are

$$\begin{aligned}&\tau=0,\quad \theta\left(R,0\right)=0\\&\tau>0,\quad R=0,\quad \frac{\partial\theta}{\partial R}=0\\&\tau>0,\quad R=1,\quad \frac{\partial\theta}{\partial R}=Bi_m\theta+Bi_r\left[\left(\theta+\varphi\right)^4-\varphi^4\right]\end{aligned} \tag{22}$$

Furthermore, the heat transfer model for the spherical-shaped particle is developed in dimensionless form is given as

$$\left(1+\lambda\left(\theta\left(R,\tau\right)+\varphi\right)\right)\frac{\partial\theta\left(R,\tau\right)}{\partial\tau}=\left(1+\zeta\left(\theta\left(R,\tau\right)+\varphi\right)\right)\frac{\partial^2\theta\left(R,\tau\right)}{\partial R^2}$$
$$+\zeta\left(\frac{\partial\theta\left(R,\tau\right)}{\partial R}\right)^2+\frac{2\left(1+\zeta\left(\theta\left(R,\tau\right)+\varphi\right)\right)}{R}\frac{\partial\theta\left(R,\tau\right)}{\partial R}-\alpha\left\{\begin{bmatrix}\beta_0+\beta_1\theta\left(R,\tau\right)+\beta_2\theta^2\left(R,\tau\right)\\+\beta_3\theta^3\left(R,\tau\right)+\beta_4\theta^4\left(R,\tau\right)\end{bmatrix}C_B\left(\tau\right)\right.$$
$$\left.+\begin{bmatrix}\gamma_0+\gamma_1\theta\left(R,\tau\right)+\gamma_2\theta^2\left(R,\tau\right)\\+\gamma_3\theta^3\left(R,\tau\right)+\gamma_4\theta^4\left(R,\tau\right)\end{bmatrix}C_T\left(\tau\right)\right\} \tag{23}$$

The initial and boundary conditions are

$$\begin{aligned} &\tau = 0, \quad \theta(R,0) = 0 \\ &\tau > 0, \quad R = 0, \quad \frac{\partial \theta}{\partial R} = 0 \\ &\tau > 0, \quad R = 1, \quad \frac{\partial \theta}{\partial R} = Bi_m \theta + Bi_r \left[ (\theta + \varphi)^4 - \varphi^4 \right] \end{aligned} \tag{24}$$

## 3 Method of Solution: Differential Transform Method

Following the introduction of differential transformation method (DTM by Zhou [66], the applications of DTM to both linear and non-linear differential and system of differential equation have fast gained ground as it has appeared in many engineering and scientific research [67-73]. The potentiality of the method is displayed in the provisions of symbolic or analytical solutions to both linear and non-linear integral and differential equations without linearization, discretization or perturbation [67-73]. DTM is capable of greatly reducing the size of computational work while still accurately providing the series solution with fast convergence rate. The basic definitions and the operational properties of the method are as follows:
If $u(t)$ is analytic in the domain T, then the function $u(t)$ will be differentiated continuously with respect to time *t.*

$$\frac{d^p u(t)}{dt^p} = \varphi(t, p) \quad \text{for all } t \in T \tag{25}$$

for $t = t_i$, then $\varphi(t, p) = \varphi(t_i, p)$ , where $p$ belongs to the set of non-negative integers, denoted as the $p$-domain. We can therefore write Eq. (25) as

$$U(p) = \varphi(t_i, p) = \left[ \frac{d^p u(t)}{dt^p} \right]_{t=t_i} \tag{26}$$

Where $U_p$ is called the spectrum of $u(t)$ at $t = t_i$

Expressing $u(t)$ in Taylor's series as

$$u(t) = \sum_p^{\infty} \left[ \frac{(t - t_i)^p}{p!} \right] U(p) \tag{27}$$

where Equ. (27) is the inverse of $U(k)$ . The symbol 'D' denoting the differential transformation process and combining (26) and (27), we have

$$u(t) = \sum_{p=0}^{\infty} \left[ \frac{(t - t_i)^p}{p!} \right] U(p) = D^{-1} U(p) \tag{28}$$

Using the operational properties of the differential transformation method, the following recursive relations for Eqs. (1a)-(1d) under isothermal condition are developed

$$C_B(p+1) = -\frac{k_1 + k_2 + k_3}{(p+1)} C_B(p) \tag{29a}$$

$$C_T(p+1)=\frac{k_2}{(p+1)}C_B(p)-\frac{\varepsilon(k_4+k_5)}{(p+1)}C_T(p) \tag{29b}$$

$$C_C(p+1)=\frac{k_3}{(p+1)}C_B(p)+\frac{\varepsilon k_5}{(p+1)}C_T(p) \tag{29c}$$

$$C_G(p+1)=\frac{k_1}{(p+1)}C_B(p)+\frac{\varepsilon k_4}{(p+1)}C_T(p) \tag{29d}$$

The differential transformation for the heat transfer model for the rectangular shaped particle as shown in Eq. (19) is

$$\begin{aligned}
&(n,p+1)\theta(n,p+1)+\lambda\sum_{r=0}^{n}\sum_{v=0}^{p}\theta(n-r,p)\left(p-v+1\right)\theta\left(r,p-v+1\right)+\lambda\varphi(n,p+1)\theta(n,p+1)=\\
&(n+1)(n+2)\theta(n+2,p)+\zeta\sum_{r=0}^{n}\sum_{v=0}^{p}\theta(r,p-v)\left(n-r+2\right)\theta\left(n-r+2,v\right)\\
&+\zeta\varphi(n+1)(n+2)\theta(n+2,p)+\zeta\sum_{r=0}^{n}\sum_{v=0}^{p}\left(v+1\right)\left(n-r+1\right)\theta(r+1,p-v)\theta\left(n-r+1,v\right)\\
&-\alpha\left\{\begin{array}{l}
\beta_o C_B\left(p\right)+\beta_1\sum_{r=0}^{n}\sum_{v=0}^{p}\theta(r,p-v)C_B\left(p\right)\\
+\beta_2\sum_{r=0}^{n}\sum_{s=0}^{u-r}\sum_{v=0}^{p}\sum_{w=0}^{p-v}\theta\left(r,p-v-w\right)\theta(s,v)C_B\left(w\right)\\
+\beta_3\sum_{r=0}^{n}\sum_{s=0}^{u-r}\sum_{q=0}^{u-r-s}\sum_{v=0}^{p}\sum_{w=0}^{p-v}\sum_{y=0}^{p-v-w}\left[\theta\left(r,p-v-w-y\right)\theta(s,v)\theta\left(q,w\right)C_B\left(w\right)\right]\\
+\beta_4\sum_{r=0}^{n}\sum_{s=0}^{u-r}\sum_{q=0}^{u-r-s}\sum_{m=0}^{u-r-s-q}\sum_{v=0}^{p}\sum_{w=0}^{p-v}\sum_{y=0}^{p-v-w}\sum_{z=0}^{p-v-w-y}\left[\begin{array}{l}\theta\left(r,p-v-w-y-z\right)\theta\left(s,v\right)\\ \cdot\theta(q,w)\theta(m,y)C_B\left(y\right)\end{array}\right]
\end{array}\right\}\\
&\left\{\begin{array}{l}
\gamma_o C_T\left(p\right)+\gamma_1\sum_{r=0}^{n}\sum_{s=0}^{p}\theta(r,p-s)C_T\left(p\right)\\
+\gamma_2\sum_{r=0}^{n}\sum_{s=0}^{u-r}\sum_{v=0}^{p}\sum_{w=0}^{p-v}\theta\left(r,p-v-w\right)\theta(s,v)C_T\left(w\right)\\
+\gamma_3\sum_{r=0}^{n}\sum_{s=0}^{u-r}\sum_{q=0}^{u-r-s}\sum_{v=0}^{p}\sum_{w=0}^{p-v}\sum_{y=0}^{p-v-w}\left[\theta\left(r,p-v-w-y\right)\theta(s,v)\theta\left(q,w\right)C_T\left(y\right)\right]\\
+\gamma_4\sum_{r=0}^{n}\sum_{s=0}^{u-r}\sum_{q=0}^{u-r-s}\sum_{m=0}^{u-r-s-q}\sum_{v=0}^{p}\sum_{w=0}^{p-v}\sum_{y=0}^{p-v-w}\sum_{z=0}^{p-v-w-y}\left[\begin{array}{l}\theta\left(r,p-v-w-y-z\right)\theta\left(s,v\right)\\ \cdot\theta(q,w)\theta(m,y)C_T\left(z\right)\end{array}\right]
\end{array}\right\}
\end{aligned} \tag{30}$$

And DTM of the initial and boundary conditions are

$$\theta(n,0)=0 \tag{31}$$

$$\left(n+1\right)\theta(0,p)=0 \tag{32}$$

The differential transformation of the second boundary condition could be written as

$$\begin{aligned}
&\sum_{r=0}^{\infty}\sum_{v=0}^{p}(r+1)\theta(r+1,p)=-Bi_m\sum_{r=0}^{\infty}\sum_{v=0}^{p}\theta(r,p)\\
&-Bi_r\sum_{r=0}^{\infty}\sum_{s=0}^{\infty}\sum_{q=0}^{\infty}\sum_{m=0}^{\infty}\sum_{v=0}^{p}\sum_{w=0}^{p-v}\sum_{y=0}^{p-v-w}\sum_{z=0}^{p-v-w-y}\left[\theta(r,p-v-w-y)\theta(s,v)\theta(q,w)\theta(r-s,y)\right]\\
&-4\varphi Bi_r\sum_{r=0}^{\infty}\sum_{s=0}^{\infty}\sum_{q=0}^{\infty}\sum_{v=0}^{p}\sum_{w=0}^{p-v}\sum_{y=0}^{p-v-w}\left[\theta(r,p-v-w)\theta(s,v)\theta(u-r-s,w)\right]\\
&-6\varphi^2 Bi_r\sum_{r=0}^{\infty}\sum_{s=0}^{\infty}\sum_{v=0}^{p}\sum_{w=0}^{p-v}\theta(r,p-v-w)\theta(s,v)-4Bi_r\varphi^3\sum_{r=0}^{n}\sum_{v=0}^{p}\theta(r,p)
\end{aligned}\tag{33}$$

The above complications in the analysis of the developed differential transformation for the secondary boundary conditions can easily be avoided and actually represented by stating that

$$\theta(1,p)=a \tag{34}$$

where "$a$" is an unknown parameter which will be found later by imposing the second boundary conditions after the algebraic solution of the thermal model.

Also, the differential transformation for the heat transfer model for the cylindrical shaped particle as shown in Eq. (21) is

$$\begin{aligned}
&\sum_{r=0}^{n}\sum_{v=0}^{p}\delta(v-1,p-v)(p-v+1)\theta(n,p-v+1)\\
&+\lambda\sum_{r=0}^{n}\sum_{s=0}^{n-r}\sum_{v=0}^{p}\sum_{w=0}^{p-v}\delta(r-1,p-v-w)\theta(n-r-s,v)(p-v-w+1)\theta(s,p-v-w+1)\\
&\lambda\varphi\sum_{r=0}^{n}\sum_{v=0}^{p}\delta(v-1,p-v)(p-v+1)\theta(n,p-v+1)=\\
&\sum_{r=0}^{n}\sum_{v=0}^{p}\delta(v-1,p-v)(p-v+1)(p-v+2)\theta(n-r+2,v)\\
&+\zeta\sum_{r=0}^{n}\sum_{s=0}^{n-r}\sum_{v=0}^{p}\sum_{w=0}^{p-v}\delta(r-1,p-v-w)\theta(r,p-v-w)(n-r-s+1)(n-r-s+2)\theta(n-r-s+2,v)\\
&+\zeta\varphi\sum_{r=0}^{n}\sum_{s=0}^{n-r}\sum_{v=0}^{p}\sum_{w=0}^{p-v}\delta(r-1,p-v)(n-r-s+1)(n-r-s+2)\theta(n-r-s+2,v)\\
&\zeta\sum_{r=0}^{n}\sum_{s=0}^{n-r}\sum_{v=0}^{p}\sum_{w=0}^{p-v}\delta(r-1,p-v-w)(v+1)(n-r-s+1)\theta(r+1,p-v-w)\theta(n-r-s+1,w)\\
&(n+1)\theta(n+1,p)+\zeta\sum_{r=0}^{n}\sum_{v=0}^{p}\delta(v-1,p-v)(n-r+1)\theta(n-r+1,v)+\zeta\varphi(n+1)\theta(n+1,p)\\
&-\alpha\left\{\begin{array}{l}
\beta_o\sum_{r=0}^{n}\sum_{v=0}^{p}\delta(r-1,p-v)C_B(p)+\beta_1\sum_{r=0}^{n}\sum_{v=0}^{p}\theta(r-1,p-v)C_B(p)\\
+\beta_2\sum_{r=0}^{n}\sum_{s=0}^{u-r}\sum_{v=0}^{p}\sum_{w=0}^{p-v}\theta(r-1,p-v-w)\theta(s,v)C_B(w)\\
+\beta_3\sum_{r=0}^{n}\sum_{s=0}^{u-r}\sum_{q=0}^{u-r-s}\sum_{v=0}^{p}\sum_{w=0}^{p-v}\sum_{y=0}^{p-v-w}\left[\theta(r-1,p-v-w-y)\theta(s,v)\theta(q,w)C_B(w)\right]\\
+\beta_4\sum_{r=0}^{n}\sum_{s=0}^{u-r}\sum_{q=0}^{u-r-s}\sum_{m=0}^{u-r-s-q}\sum_{v=0}^{p}\sum_{w=0}^{p-v}\sum_{y=0}^{p-v-w}\sum_{z=0}^{p-v-w-y}\left[\begin{array}{l}\theta(r-1,p-v-w-y-z)\theta(s,v)\\ \cdot\theta(q,w)\theta(m,y)C_B(y)\end{array}\right]
\end{array}\right\}\\
&\left\{\begin{array}{l}
\gamma_o\sum_{r=0}^{n}\sum_{s=0}^{p}\delta(r-1,p-s)C_T(p)+\gamma_1\sum_{r=0}^{n}\sum_{s=0}^{p}\theta(r-1,p-s)C_T(p)\\
+\gamma_2\sum_{r=0}^{n}\sum_{s=0}^{u-r}\sum_{v=0}^{p}\sum_{w=0}^{p-v}\theta(r-1,p-v-w)\theta(s,v)C_T(w)\\
+\gamma_3\sum_{r=0}^{n}\sum_{s=0}^{u-r}\sum_{q=0}^{u-r-s}\sum_{v=0}^{p}\sum_{w=0}^{p-v}\sum_{y=0}^{p-v-w}\left[\theta(r-1,p-v-w-y)\theta(s,v)\theta(q,w)C_T(y)\right]\\
+\gamma_4\sum_{r=0}^{n}\sum_{s=0}^{u-r}\sum_{q=0}^{u-r-s}\sum_{m=0}^{u-r-s-q}\sum_{v=0}^{p}\sum_{w=0}^{p-v}\sum_{y=0}^{p-v-w}\sum_{z=0}^{p-v-w-y}\left[\begin{array}{l}\theta(r-1,p-v-w-y-z)\theta(s,v)\\ \cdot\theta(q,w)\theta(m,y)C_T(z)\end{array}\right]
\end{array}\right\}
\end{aligned}\tag{35}$$

Furthermore, the differential transformation for the heat transfer model for the spherical shaped particle as shown in Eq. (23) is

$$
\begin{aligned}
&\sum_{r=0}^{n}\sum_{v=0}^{p}\delta(v-1,p-v)\left(p-v+1\right)\theta\left(n,p-v+1\right)\\
&+\lambda\sum_{r=0}^{n}\sum_{s=0}^{n-r}\sum_{v=0}^{p}\sum_{w=0}^{p-v}\delta\left(r-1,p-v-w\right)\theta\left(n-r-s,v\right)\left(p-v-w+1\right)\theta\left(s,p-v-w+1\right)\\
&\lambda\varphi\sum_{r=0}^{n}\sum_{v=0}^{p}\delta(v-1,p-v)\left(p-v+1\right)\theta\left(n,p-v+1\right)=\\
&\sum_{r=0}^{n}\sum_{v=0}^{p}\delta(v-1,p-v)\left(p-v+1\right)\left(p-v+2\right)\theta\left(n-r+2,v\right)\\
&+\zeta\sum_{r=0}^{n}\sum_{s=0}^{n-r}\sum_{v=0}^{p}\sum_{w=0}^{p-v}\delta\left(r-1,p-v-w\right)\theta\left(r,p-v-w\right)\left(n-r-s+1\right)\left(n-r-s+2\right)\theta\left(n-r-s+2,v\right)\\
&+\zeta\varphi\sum_{r=0}^{n}\sum_{s=0}^{n-r}\sum_{v=0}^{p}\sum_{w=0}^{p-v}\delta\left(r-1,p-v\right)\left(n-r-s+1\right)\left(n-r-s+2\right)\theta\left(n-r-s+2,v\right)\\
&\zeta\sum_{r=0}^{n}\sum_{s=0}^{n-r}\sum_{v=0}^{p}\sum_{w=0}^{p-v}\delta\left(r-1,p-v-w\right)\left(v+1\right)\left(n-r-s+1\right)\theta\left(r+1,p-v-w\right)\theta\left(n-r-s+1,w\right)\\
&2(n+1)\theta(n+1,p)+2\zeta\sum_{r=0}^{n}\sum_{v=0}^{p}\delta(v-1,p-v)\left(n-r+1\right)\theta\left(n-r+1,v\right)+2\zeta\varphi(n+1)\theta(n+1,p)\\
&-\alpha\left\{\begin{array}{l}
\beta_o\sum_{r=0}^{n}\sum_{v=0}^{p}\delta(r-1,p-v)C_B\left(p\right)+\beta_1\sum_{r=0}^{n}\sum_{v=0}^{p}\theta(r-1,p-v)C_B\left(p\right)\\
+\beta_2\sum_{r=0}^{n}\sum_{s=0}^{u-r}\sum_{v=0}^{p}\sum_{w=0}^{p-v}\theta\left(r-1,p-v-w\right)\theta(s,v)C_B\left(w\right)\\
+\beta_3\sum_{r=0}^{n}\sum_{s=0}^{u-r}\sum_{q=0}^{u-r-s}\sum_{v=0}^{p}\sum_{w=0}^{p-v}\sum_{y=0}^{p-v-w}\left[\theta\left(r-1,p-v-w-y\right)\theta(s,v)\theta\left(q,w\right)C_B\left(w\right)\right]\\
+\beta_4\sum_{r=0}^{n}\sum_{s=0}^{u-r}\sum_{q=0}^{u-r-s}\sum_{m=0}^{u-r-s-q}\sum_{v=0}^{p}\sum_{w=0}^{p-v}\sum_{y=0}^{p-v-w}\sum_{z=0}^{p-v-w-y}\left[\begin{array}{l}\theta\left(r-1,p-v-w-y-z\right)\theta\left(s,v\right)\\ \cdot\theta(q,w)\theta(m,y)C_B\left(y\right)\end{array}\right]
\end{array}\right\}\\
&\left\{\begin{array}{l}
\gamma_o\sum_{r=0}^{n}\sum_{s=0}^{p}\delta(r-1,p-s)C_T\left(p\right)+\gamma_1\sum_{r=0}^{n}\sum_{s=0}^{p}\theta(r-1,p-s)C_T\left(p\right)\\
+\gamma_2\sum_{r=0}^{n}\sum_{s=0}^{u-r}\sum_{v=0}^{p}\sum_{w=0}^{p-v}\theta\left(r-1,p-v-w\right)\theta(s,v)C_T\left(w\right)\\
+\gamma_3\sum_{r=0}^{n}\sum_{s=0}^{u-r}\sum_{q=0}^{u-r-s}\sum_{v=0}^{p}\sum_{w=0}^{p-v}\sum_{y=0}^{p-v-w}\left[\theta\left(r-1,p-v-w-y\right)\theta(s,v)\theta\left(q,w\right)C_T\left(y\right)\right]\\
+\gamma_4\sum_{r=0}^{n}\sum_{s=0}^{u-r}\sum_{q=0}^{u-r-s}\sum_{m=0}^{u-r-s-q}\sum_{v=0}^{p}\sum_{w=0}^{p-v}\sum_{y=0}^{p-v-w}\sum_{z=0}^{p-v-w-y}\left[\begin{array}{l}\theta\left(r-1,p-v-w-y-z\right)\theta\left(s,v\right)\\ \cdot\theta(q,w)\theta(m,y)C_T\left(z\right)\end{array}\right]
\end{array}\right\}
\end{aligned}
\tag{36}
$$

It should be noted that the differential transformed of initial and boundary conditions for cylindrical and spherical shapes are identical and equivalent to that of rectangular shaped particle as presented in Eqs. (31), (32) and (34). The solutions of the kinetic equations for the isothermal condition are given as follows:

**The analysis of $C_B(p+1)$:**

From Equ. (29a), we have

$$C_B(p+1)=\frac{-(k_1+k_2+k_3)}{p+1}C_B(p)$$

Analyzing the differential transform in Eq. (29), we have

$$C_B(1) = -(k_1 + k_2 + k_3)C_{Bo},\ \ C_B(2) = \frac{(k_1 + k_2 + k_3)^2}{2} C_{Bo},\qquad C_B(3) = \frac{-(k_1 + k_2 + k_3)^3}{6} C_{Bo}$$

$$C_B(4) = \frac{(k_1 + k_2 + k_3)^4}{24} C_{Bo},\ C_B(5) = \frac{-(k_1 + k_2 + k_3)^5}{120} C_{Bo},\qquad C_B(6) = \frac{(k_1 + k_2 + k_3)^6}{720} C_{Bo}$$

$$C_B(7) = \frac{-(k_1 + k_2 + k_3)^7}{5040} C_{Bo},\ \ C_B(8) = \frac{(k_1 + k_2 + k_3)^8}{40,320} C_{Bo},\cdots\ C(n) = (-1)^n \frac{(k_1 + k_2 + k_3)^n}{n!} C_{Bo}$$

Applying the inverse differential transform,

$$\begin{aligned} C_B(t) &= C_B(0) + C_B(1)t + C_B(2)t^2 + C_B(3)t^3 \\ &\quad + C_B(4)t^4 + C_B(5)t^5 + C_B(6)t^6 + C_B(7)t^7 + C_B(8)t^8 + \ldots + C_B(n)t^n \end{aligned} \tag{37}$$

After substituting the results in the above analysis into Eq. (37), we have

$$\begin{aligned} C_B(t) = C_{Bo} &- \left[(k_1 + k_2 + k_3)\right]C_{Bo}t + \left[\frac{(k_1 + k_2 + k_3)}{2}\right]C_{Bo}t^2 - \left[\frac{(k_1 + k_2 + k_3)^3}{6}\right]C_{Bo}t^3 + \left[\frac{(k_1 + k_2 + k)^4}{24}\right]C_{Bo}t^4 \\ &- \left[\frac{(k_1 + k_2 + k_3)^5}{120}\right]C_{Bo}t^5 + \frac{(k_1 + k_2 + k_3)6}{720}C_{Bo}t^6 - \left[\frac{(k_1 + k_2 + k_3)^7}{5040}\right]C_{Bo}t^7 + \left[\frac{(k_1 + k_2 + k_3)^8}{40,320}\right]C_{Bo}t^8 \\ &- \left[\frac{(k_1 + k_2 + k_3)^9}{362880}\right]C_{Bo}t^9 + \left[\frac{(k_1 + k_2 + k_3)^{10}}{3628800}\right]C_{Bo}t^{10} - \left[\frac{(k_1 + k_2 + k_3)^{11}}{39916800}\right]C_{Bo}t^{11} + \left[\frac{(k_1 + k_2 + k_3)^{12}}{479001600}\right]C_{Bo}t^{12} \\ &- \left[\frac{(k_1 + k_2 + k_3)}{6227020800}\right]C_{Bo}t^{13} + \left[\frac{(k_1 + k_2 + k_3)}{87178291200}\right]C_{Bo}t^{14} - \left[\frac{(k_1 + k_2 + k_3)}{1307674368000}\right]C_{Bo}t^{15} + \ldots \end{aligned} \tag{38}$$

Eq. (38) can be written as

$$C_B(t) = C_{Bo}\left[\begin{aligned} &1 - (k_1 + k_2 + k_2)t + \frac{(k_1 + k_2 + k_2)^2}{2}t^2 - \frac{(k_1 + k_2 + k_3)^3}{6}t^3 + \frac{(k_1 + k_2 + k_3)^4}{24}t^4 \\ &- \frac{(k_1 + k_2 + k_3)^5}{120}t^5 + \frac{(k_1 + k_2 + k_3)^6}{720}t^6 - \frac{(k_1 + k_2 + k_3)^7}{5040}t^7 + \frac{(k_1 + k_2 + k_3)^8}{40320}t^8 \\ &- \frac{(k_1 + k_2 + k_3)^9}{362880}t^9 + .\frac{(k_1 + k_2 + k_3)^{10}}{3628800}t^{10} - \frac{(k_1 + k_2 + k_3)^{11}}{39916800}t^{11} + \frac{(k_1 + k_2 + k_3)^{12}}{479001600}t^{12} \\ &- \frac{(k_1 + k_2 + k_3)^{13}}{6227020800}t^{13} + \frac{(k_1 + k_2 + k_3)^{14}}{87178291200}t^{14} - \frac{(k_1 + k_2 + k_3)}{1307674368000}t^{15} + \ldots \end{aligned}\right] \tag{39}$$

$$C_{B0}(t) = C_{Bo}\sum_{p=0}^{N}\frac{(-1)^p}{p!}(k_1 + k_2 + k_3)^p t^p = C_{Bo}\,\mathrm{e}^{-((k_1+k_2+k_3)t)} \tag{40}$$

**The analysis of $C_T(p+1)$:**

From Equ. (29b)

$$C_T(p+1)=\frac{k_2}{(p+1)}C_B(p)-\frac{\varepsilon(k_4+k_5)}{(p+1)}C_T(p)$$

On analyzing the differential transform in Eq. (29b), we have

$$C_T(1)=k_2C_{Bo}$$

$$C_T(2)=-\left\{\frac{k_2(k_1+k_2+k_3)}{2}+\frac{\varepsilon k_2(k_4+k_5)}{2}\right\}C_{Bo}$$

$$C_T(3)=\left\{\frac{k_2(k_1+k_2+k_3)^2}{3}+\left\{\varepsilon k_2(k_4+k_5)\left[\frac{(k_1+k_2+k_3)}{6}+\frac{[\varepsilon(k_4+k_5)]^2}{6}\right]\right\}\right\}C_{Bo}$$

$$C_T(4)=-\left\{\frac{k_2(k_1+k_2+k_3)^3}{24}+\frac{\varepsilon(k_4+k_5)}{4}\left\{\begin{array}{l}\dfrac{k_2(k_1+k_2+k_3)^2}{3}\\ +\left\{\varepsilon k_2(k_4+k_5)\left[\begin{array}{l}\dfrac{(k_1+k_2+k_3)}{6}\\ +\dfrac{[\varepsilon(k_4+k_5)]^2}{6}\end{array}\right]\right\}\end{array}\right\}\right\}C_{Bo}$$

$$C_T(5)=\left\{\frac{k_2(k_1+k_2+k_3)^4}{120}+\frac{\varepsilon(k_4+k_5)}{5}\left\{\begin{array}{l}\dfrac{k_2(k_1+k_2+k_3)^3}{24}\\ +\dfrac{\varepsilon(k_4+k_5)}{4}\left\{\begin{array}{l}\dfrac{k_2(k_1+k_2+k_3)^2}{3}\\ +\left\{\varepsilon k_2(k_4+k_5)\left[\begin{array}{l}\dfrac{(k_1+k_2+k_3)}{6}\\ +\dfrac{[\varepsilon(k_4+k_5)]^2}{6}\end{array}\right]\right\}\end{array}\right\}\end{array}\right\}\right\}C_{Bo}$$

$$C_T(6)=-\left\{\begin{array}{l}\dfrac{k_2(k_1+k_2+k_3)^5}{720}\\ +\dfrac{\varepsilon(k_4+k_5)}{6}\left\{\begin{array}{l}\dfrac{k_2(k_1+k_2+k_3)^4}{120}\\ +\dfrac{\varepsilon(k_4+k_5)}{5}\left\{\begin{array}{l}\dfrac{k_2(k_1+k_2+k_3)^3}{24}\\ +\dfrac{\varepsilon(k_4+k_5)}{4}\left\{\begin{array}{l}\dfrac{k_2(k_1+k_2+k_3)^2}{3}\\ +\left\{\varepsilon k_2(k_4+k_5)\left[\begin{array}{l}\dfrac{(k_1+k_2+k_3)}{6}\\ +\dfrac{[\varepsilon(k_4+k_5)]^2}{6}\end{array}\right]\right\}\end{array}\right\}\end{array}\right\}\end{array}\right\}\end{array}\right\}C_{Bo}$$

and so on. Therefore, the differential transformation solution of $C_T$ is given as

$$C_T(t) = C_T(0) + C_T(1)t + C_T(2)t^2 + C_T(3)t^3 + C_T(4)t^4 + C_T(5)t^5 + C_T(6)t^6 + ... + C_T(n)t^n \quad (41)$$

**The analysis of $C_C(p+1)$:**

From Equ. (29c)

$$C_C(p+1) = \frac{k_3}{(p+1)} C_B(p) + \frac{\varepsilon k_5}{(p+1)} C_T(p)$$

Analyzing Eq. (26c) as before, we have

$$C_C(1) = k_3 C_{Bo},$$

$$C_C(2) = -\left\{ \frac{k_3(k_1+k_2+k_3)}{2} - \frac{\varepsilon k_3 k_5}{2} \right\} C_{Bo}$$

$$C_C(3) = \left\{ \frac{k_3(k_1+k_2+k_3)^2}{3} - \left\{ \varepsilon k_3 k_5 \left[ \frac{(k_1+k_2+k_3)}{6} + \frac{[\varepsilon k_3 k_5]^2}{6} \right] \right\} \right\} C_{Bo}$$

$$C_C(4) = -\left\{ \frac{k_3(k_1+k_2+k_3)^3}{24} - \frac{\varepsilon k_3 k_5}{4} \left\{ \begin{array}{l} \frac{k_3(k_1+k_2+k_3)^2}{3} \\ + \left\{ \varepsilon k_3 k_5 \left[ \begin{array}{l} \frac{(k_1+k_2+k_3)}{6} \\ + \frac{(\varepsilon k_3 k_5)^2}{6} \end{array} \right] \right\} \end{array} \right\} \right\} C_{Bo}$$

$$C_C(5) = \left\{ \frac{k_3(k_1+k_2+k_3)^4}{120} - \frac{\varepsilon k_3 k_5}{5} \left\{ \begin{array}{l} \frac{k_3(k_1+k_2+k_3)^3}{24} \\ - \frac{\varepsilon k_3 k_5}{4} \left\{ \begin{array}{l} \frac{k_3(k_1+k_2+k_3)^2}{3} \\ - \left\{ \varepsilon k_3 k_5 \left[ \begin{array}{l} \frac{(k_1+k_2+k_3)}{6} \\ - \frac{(\varepsilon k_3 k_5)^2}{6} \end{array} \right] \right\} \end{array} \right\} \end{array} \right\} \right\} C_{Bo}$$

$$C_C(6) = -\left\{ \begin{array}{l} \frac{k_3(k_1+k_2+k_3)^5}{720} \\ - \frac{\varepsilon k_3 k_5}{6} \left\{ \frac{k_3(k_1+k_2+k_3)^4}{120} - \frac{\varepsilon k_3 k_5}{5} \left\{ \begin{array}{l} \frac{k_3(k_1+k_2+k_3)^3}{24} \\ - \frac{\varepsilon k_3 k_5}{4} \left\{ \begin{array}{l} \frac{k_3(k_1+k_2+k_3)^2}{3} \\ - \left\{ \varepsilon k_3 k_5 \left[ \begin{array}{l} \frac{(k_1+k_2+k_3)}{6} \\ - \frac{(\varepsilon k_3 k_5)^2}{6} \end{array} \right] \right\} \end{array} \right\} \end{array} \right\} \right\} \end{array} \right\} C_{Bo}$$

and so on. The differential transformation solution of $C_C$ is given as

$$C_C(t) = C_C(0) + C_C(1)t + C_C(2)t^2 + C_C(3)t^3 + C_C(4)t^4 + C_C(5)t^5 + C_C(6)t^6 + ... + C_C(n)t^n \quad (42)$$

**The analysis of $C_C(p+1)$:**

From Equ. (29d)

$$C_G(p+1) = \frac{k_1}{(p+1)} C_B(p) + \frac{\varepsilon k_4}{(p+1)} C_T(p)$$

On analyzing Eq. (29d) as before, we have

$$C_G(1) = k_1 C_{Bo}$$

$$C_G(2) = -\left\{ \frac{k_1(k_1+k_2+k_3)}{2} - \frac{\varepsilon k_1 k_4}{2} \right\} C_{Bo}$$

$$C_G(3) = \left\{ \frac{k_1(k_1+k_2+k_3)^2}{3} - \left\{ \varepsilon k_1 k_4 \left[ \frac{(k_1+k_2+k_3)}{6} + \frac{(\varepsilon k_1 k_4)^2}{6} \right] \right\} \right\} C_{Bo}$$

$$C_G(4) = -\left\{ \frac{k_1(k_1+k_2+k_3)^3}{24} - \frac{\varepsilon k_1 k_4}{4} \left\{ \frac{k_1(k_1+k_2+k_3)^2}{3} + \left\{ \varepsilon k_1 k_4 \left[ \frac{(k_1+k_2+k_3)}{6} + \frac{(\varepsilon k_1 k_4)^2}{6} \right] \right\} \right\} \right\} C_{Bo}$$

$$C_G(5) = \left\{ \frac{k_1(k_1+k_2+k_3)^4}{120} - \frac{\varepsilon k_1 k_4}{5} \left\{ \frac{k_1(k_1+k_2+k_3)^3}{24} - \frac{\varepsilon k_1 k_4}{4} \left\{ \frac{k_1(k_1+k_2+k_3)^2}{3} - \left\{ \varepsilon k_1 k_4 \left[ \frac{(k_1+k_2+k_3)}{6} - \frac{(\varepsilon k_1 k_4)^2}{6} \right] \right\} \right\} \right\} \right\} C_{Bo}$$

$$C_G(6) = -\left\{ \frac{k_1(k_1+k_2+k_3)^5}{720} - \frac{\varepsilon k_1 k_4}{6} \left\{ \frac{k_1(k_1+k_2+k_3)^4}{120} - \frac{\varepsilon k_1 k_4}{5} \left\{ \frac{k_1(k_1+k_2+k_3)^3}{24} - \frac{\varepsilon k_1 k_4}{4} \left\{ \frac{k_1(k_1+k_2+k_3)^2}{3} - \left\{ \varepsilon k_1 k_4 \left[ \frac{(k_1+k_2+k_3)}{6} - \frac{(\varepsilon k_1 k_4)^2}{6} \right] \right\} \right\} \right\} \right\} \right\} C_{Bo}$$

and so on. The differential transformation solution of $C_C$ is given as

$$C_G(t) = C_G(0) + C_G(1)t + C_G(2)t^2 + C_G(3)t^3 + C_G(4)t^4 + C_G(5)t^5 + C_G(6)t^6 + ... + C_G(n)t^n \quad (43)$$

The above step by step solutions of the kinetics equations as shown during the analysis of the solutions presented in Eq. (40)-(44) are correspondingly coupled with the solutions of differential transformation of the thermal models presented in Eq. (30), (35) and (36). The coupled equations in differential transformation forms are solved using the initial and the boundary conditions in Eqs. (31), (32) and (34). The solutions are too long to be included in this paper. However, the results are presented in the following section of results and discussion.

For the purpose of verifying the solution of the differential transformation method, exact analytical solutions using Laplace transform have been developed for Eqs. (1a)-(1d) subject to isothermal condition as

$$C_B = C_{Bo}\, \mathrm{e}^{-((k_1+k_2+k_3)t)} \quad (44a)$$

$$C_T = \frac{k_2 C_{Bo}\left[\mathrm{e}^{-((k_1+k_2+k_3)t)} - \mathrm{e}^{-\varepsilon((k_4+k_5)t)}\right]}{\varepsilon(k_4+k_5)-(k_1+k_2+k_3)} \quad (44b)$$

$$C_C = \left\{ \frac{k_3\left(1-\mathrm{e}^{-((k_1+k_2+k_3)t)}\right)}{(k_1+k_2+k_3)} - \frac{\varepsilon k_2 k_5\left[\frac{\left(1-\mathrm{e}^{-((k_1+k_2+k_3)t)}\right)}{\left(k_1+k_2+k_3\right)} + \frac{\left(1-\mathrm{e}^{-(\varepsilon(k_4+k_5)t)}\right)}{\varepsilon(k_4+k_5)}\right]}{\varepsilon(k_4+k_5)-(k_1+k_2+k_3)} \right\} C_{Bo} \quad (44c)$$

$$\theta = \frac{Bi_{mo}}{\gamma}\left\{\left[2\sum_{n=1}^{\infty}\left[\frac{\cos(\beta_n X)e^{-(\alpha\gamma+\beta_n^2)\tau}}{(\alpha\gamma+\beta_n^2)\{\cos(\beta_n)+\frac{(1+Bi_{mo})}{\beta_n}\sin(\beta_n)\}}\right] - 2\sum_{n=1}^{\infty}\left[\frac{\cos(\beta_n X)e^{-(\alpha\gamma+\beta_n^2)\tau}}{\beta_n^2\{(\cos\beta_n)+\frac{(1+Bi_{mo})}{\beta_n}\sin\beta_n\}}\right]\right] - \frac{1}{Bi_{mo}}\left[1-e^{-\alpha\gamma\tau}\right] - \frac{1}{Bi_{mo}} + \frac{\cosh\sqrt{\alpha\gamma}X}{Bi_{mo}\cosh\sqrt{\alpha\gamma}+\sqrt{\alpha\gamma}\sinh\sqrt{\alpha\gamma}}\right\} \quad (44d)$$

Also, using integral transforms, the analytical solution for the linearized form of the thermal model of the rectangular shaped particle where the outer boundary of the biomass particle is subjected to a linearized form of convective and radiative heat transfer is given as

$$C_G = \left\{ \frac{k_1\left(1-\mathrm{e}^{-((k_1+k_2+k_3)t)}\right)}{(k_1+k_2+k_3)} - \frac{\varepsilon k_2 k_4\left[\frac{\left(1-\mathrm{e}^{-((k_1+k_2+k_3)t)}\right)}{\left(k_1+k_2+k_3\right)} + \frac{\left(1-\mathrm{e}^{-(\varepsilon(k_4+k_5)t)}\right)}{\varepsilon(k_4+k_5)}\right]}{\varepsilon(k_4+k_5)-(k_1+k_2+k_3)} \right\} C_{Bo} \quad (45)$$

where $\beta_n$ are the roots of equation

$$Bi_m \cos(\beta_n) + \beta_n \sin(\beta_n) = 0$$

while the cylindrical shaped-particle, the analytical solution for the temperature distribution is given as

$$\theta = 2\left\{\left[\left[\sum_{n=1}^{\infty}\beta_n \frac{\{(\alpha J_1(\beta_n)+\beta_n^2(\beta_n^2+\alpha\lambda)\}}{(\beta_n^2+\alpha\gamma)(Bi_m+\beta_n^2)}\{\frac{J_0(\beta_n R)}{J_0^2(\beta_n)}\}e^{-(\alpha\lambda+n^2)\tau}\right]\right]\right\} \quad (46)$$
$$-\sum_{n=1}^{\infty}\left[\frac{\beta_n\{\alpha J_1(\beta_n)\}J_0(\beta_n R)}{(\beta_n^2+\alpha\lambda)(Bi_m^2+\beta_n^2)J_0^2(\beta_n)}\right]$$

where $\beta_n$ are the roots of the equation

$$J_0(\beta_n)\left[\frac{\partial\theta}{\partial R}\right]_{R=1} + J_0(\beta_n)Bi_m[\theta]_{R=1} = 0 \text{ for } for \quad \beta_n > 0$$

and $J_0(n), J_0(n\beta)\ and\ J_1(n)$ are the Bessel functions of first kind and are given by:

$$J_0(\beta)=\sum_{m=0}^{\infty}\frac{(-1)^m\beta^{2m}}{2^{2m}m!\Gamma(m+1)},\ J_0(n\beta)=\sum_{m=0}^{\infty}\frac{(-1)^m(n\lambda)^{2m}}{2^{2m}m!\Gamma(m+1)},\ J_1(\beta)=\sum_{m=0}^{\infty}\frac{(-1)^m\beta^{2m}}{2^{2m}m!\Gamma(m+2)}$$

And the spherical shaped-particle temperature distribution model is developed as

$$\theta = \frac{Bi_m}{\lambda}\left\{2\left[\sum_{n=1}^{\infty}\left[\frac{\sin(\beta_n R)e^{-(\alpha\lambda+\beta_n^2)\tau}}{(\alpha\lambda+\beta_n^2)\{(\cos\beta_n)\{\frac{Bi_m}{\beta_n}\}-\sin\beta_n\}}\right]\right]\right. \quad (47)$$
$$-(\lambda+1)\sum_{n=1}^{\infty}\left[\frac{\sin(\beta_n R)e^{-(\alpha\lambda+\beta_n^2)\tau}}{\beta_n^2\{(\cos\beta_n)\{\frac{Bi_m}{\beta_n}\}-\sin\beta_n\}}\right]$$
$$\left.-\frac{1}{Bi_m}\left[1-(\lambda+1)e^{-\alpha\lambda\tau}\right]+\frac{2\sin\sqrt{\alpha\lambda}R}{\sqrt{\alpha\lambda}\cosh\sqrt{\alpha\lambda}+(Bi_m-1)\sinh\sqrt{\alpha\lambda}}\right\}$$

where $\beta_n$ are the roots of equation

$$\beta_n\cos(\beta_n)+Bi_m\sin(\beta_n)=0$$

and

$$\alpha=\frac{\Omega_0 L^2}{K(T_f-T_0)},\ Bi_{mo}=\frac{L}{K}\left[h+\sigma\varepsilon(T^3+T_fT^2+T_f^2T+T_f^3\right],\alpha\gamma=\Omega_1(T_f-T_o)$$

$$\Omega_o=\sum_{i=1}^{3}C_B\Delta h_i A_i e^{-\frac{E_i}{R_gT_o}}+\sum_{4}^{5}C_T\Delta h_i A_i e^{-\frac{E_i}{R_gT_o}},\ \ \Omega_1=\sum_{i=1}^{3}\frac{E_i}{R_gT_o^2}C_B\Delta h_i A_i e^{-\frac{E_i}{R_gT_o}}+\sum_{4}^{5}\frac{E_i}{R_gT_o^2}C_T\Delta h_i A_i e^{-\frac{E_i}{R_gT_o}}$$

Table (1), (2), (3) and (4) present the parameters used for the simulation of the kinetic and heat transfer models.

**Table 1** Operational properties of differential transformation method

| S/N | Function | Differential transform |
|---|---|---|
| i | $u(t)\pm v(t)$ | $U(p)\pm V(p)$ |
| ii | $\alpha u(t)$ | $\alpha U(p)$ |
| iii | $\frac{du(t)}{dt}$ | $(p+1)\,U(p+1)$ |
| iv | $u(t)v(t)$ | $\sum_{r=0}^{p} V(r)U(p-r)$ |
| v | $u^m(t)$ | $\sum_{r=0}^{p} U^{m-1}(r)U(p-r)$ |
| vi | $\frac{d^n u(t)}{dx^n}$ | $(p+1)(p+2)\cdots(p+n)U(p+n)$ |
| vii | $\sin(\omega t+\alpha)$ | $\frac{\omega^p}{\mathrm{p!}}\sin\left(\frac{\pi p}{2!}+\alpha\right)$ |
| viii | $\cos(\omega t+\alpha)$ | $Z(p)=\frac{\omega^p}{\mathrm{p!}}\cos\left(\frac{\pi p}{2!}+\alpha\right)$ |

**Table 2** Values of the Parameters employed in this study

| S/N | Parameter Description | Symbol | Value used | Source |
|---|---|---|---|---|
| 1 | Bulk density of wood | ρ | 650Kg/m$^3$ | [22] |
| 2 | Thermal conductivity of wood | K | 0.1256W/mK | [1] |
| 3 | Initial thermal diffusivity of wood | α | 1.79x10$^7$m$^2$/s | [21] |
| 4 | Initial temperature of wood | $T_o$ | 303K | [1] |
| 5 | Half length of the particle | L | 0.003m | [22] |
| 6 | Convective heat transfer co-efficient | h | 8.4W/m$^2$k | [1] |
| 7 | Reactor final temperature | $T_f$ | 643K | [22] |
| 8 | Porosity of the wood particle | ε | 0.4 | [24] |
| 9 | Apparent activation energy | A | 3000/s | [1] |
| 11 | Modified Biot number | $Bi_m$ | 0.82-1.22 | Estimated |
| 12 | Specific heat capacity of wood | $C_p$ | 1670J/KgK | [1] |
| 13 | Emissivity of wood | ϵ | 0.95 | [1] |
| 14 | Stefan-Boltzmann constant | σ | 5.67x10$^8$W/m$^2$K$^4$ | [74] |
| 15 | Wood concentration | C | 650Kg/m$^3$ | [22] |

**Table 3** Kinetic constants used in the simulations

| *i* | *Reaction* | $A_i$ *(s$^{-1}$)* | $E_i$ *(kJ/mol)* | *Source* |
|---|---|---|---|---|
| 1 | Biomass→Gas | 1.3x10$^8$ | 140 | [11] |
| 2 | Biomass→Tar | 2.0x10$^8$ | 133 | [11] |
| 3 | Biomass→Char | 1.08x10$^7$ | 121 | [11] |
| 4 | Tar→Gas | 4.28x10$^6$ | 107 | [58] |
| 5 | Tar→Char | 1.0x10$^6$ | 107 | [58] |

**Table 4** Change in enthalpy values used in the simulations

| *i* | *Reaction* | $\Delta h_i$ *(kJ/kg)* | *Source* |
|---|---|---|---|
| 1 | Biomass→Gas | -418.0 | [11] |
| 2 | Biomass→Tar | -418.0 | [11] |
| 3 | Biomass→Char | -418.0 | [11] |
| 4 | Tar→Gas | 42.0 | [12] |
| 5 | Tar→Char | 42.0 | [12] |

**Table 5** Comparison of Results

| | **Temperature** | | | |
|---|---|---|---|---|
| Time | Pyle and Zaror (Exp) [1] | Jalan and Srivasta's model [21] | Babu and Chaurasia's model [23] | The Present model |
| 0 | 303 | 303 | 303 | 303 |
| 20 | 397 | 387 | 400 | 398 |
| 40 | 493 | 478 | 493 | 493 |
| 60 | 541 | 533 | 552 | 550 |
| 80 | 581 | 574 | 588 | 586 |
| 100 | 609 | 602 | 610 | 609 |
| 150 | 641 | 630 | 634 | 636 |
| 200 | 648 | 639 | 640 | 643 |

## 4 Results and Discussion

Table (5) shows the comparison of the results in the previous works and the present work. It is found that the models developed in the present study are in excellent agreement with the experimental results and the numerical solutions of the previous works.

### *4.1 Effects of isothermal heating temperature on pyrolysis yields.*

According to the two-stage parallel reaction model used in this work, as the pyrolysis zone temperature increases, the biomass undergoes thermal degradation according to primary reactions giving gas, tar and char as products. Tar also undergoes secondary reactions to give gas and char. Since the amounts of each of these products vary depending mainly on the zone temperature, the influences of heating conditions on the particle residence time and pyrolysis yield are studied using the differential transformation method.
Figs. (4-17) show the effects of isothermal heating temperatures on the particle resident time. Also, the figures demonstrate the agreement between the exact analytical solutions and the approximate analytical solutions developed by using differential transformation method.

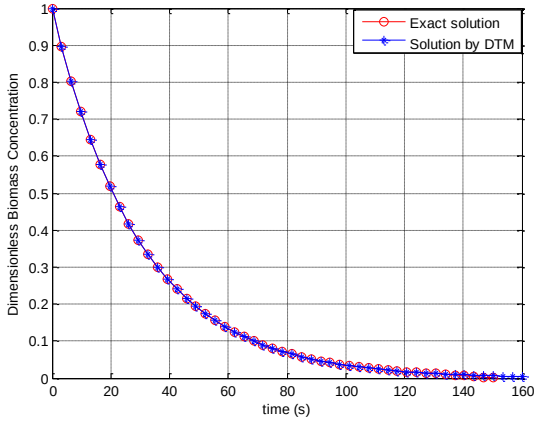


**Figure 4** Biomass concentration against time at an isothermal temperature of 673K

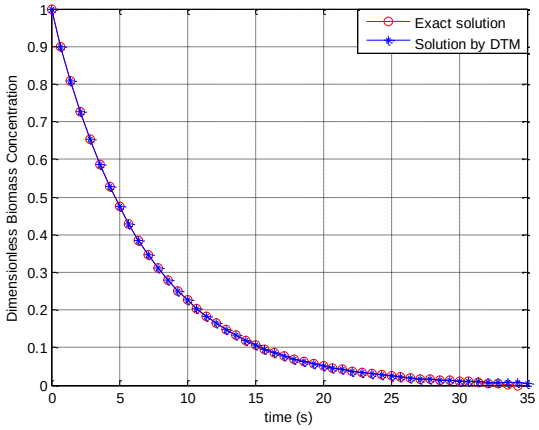


**Figure 5** Biomass concentration against time at an isothermal temperature of 773K

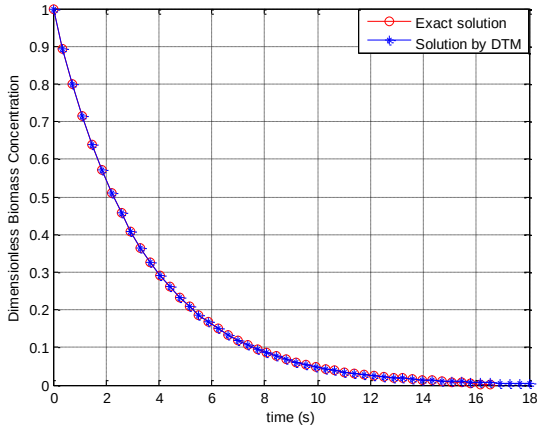


**Figure 6** Biomass concentration against time at an isothermal temperature of 873K

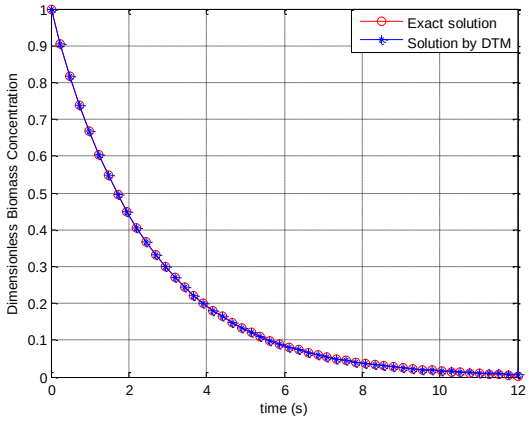


**Figure 7** Biomass concentration against time at isothermal temperature of 973K

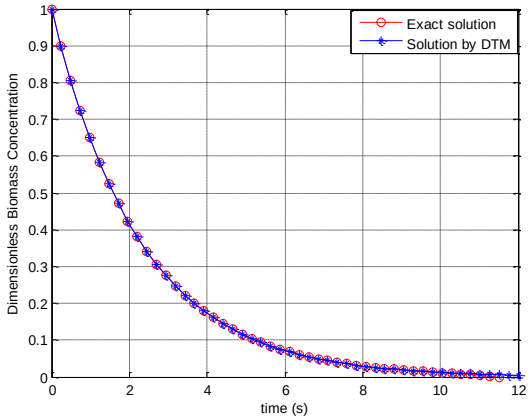


**Figure 8** Biomass concentration against time at an isothermal temperature of 1073K

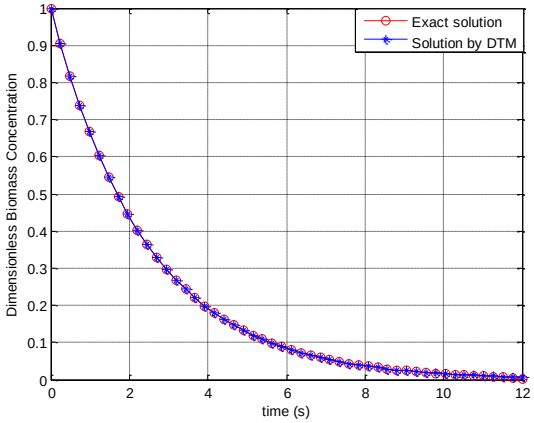


**Figure 9** Biomass concentration against time at isothermal temperature of 1173K

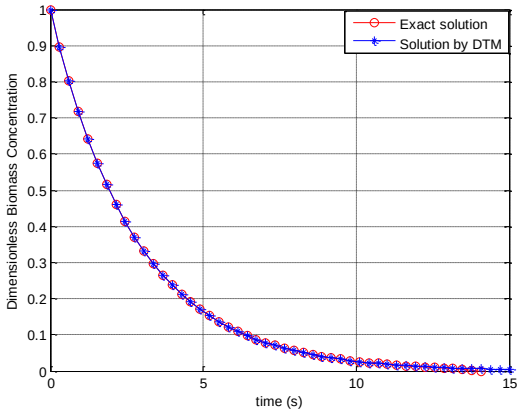


**Figure 10** Comparison of results of biomass concentration against time at an isothermal temperature of 1273K

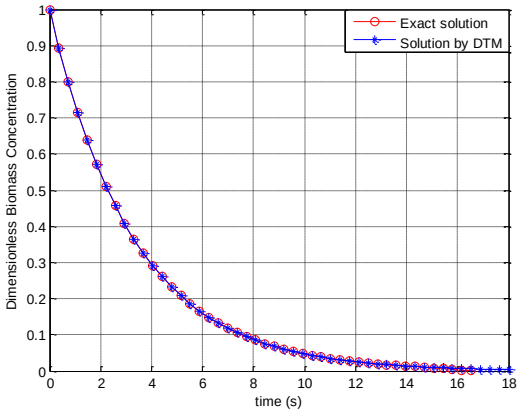


**Figure 11** Comparison of results of biomass concentration against time at isothermal temperature of 1373K

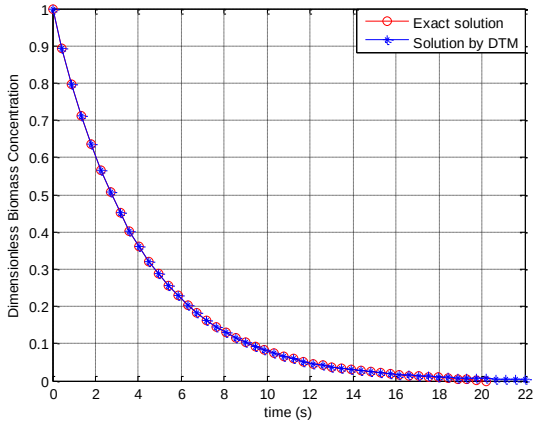


**Figure 12** Comparison of results of biomass concentration against time at an isothermal temperature of 1473K

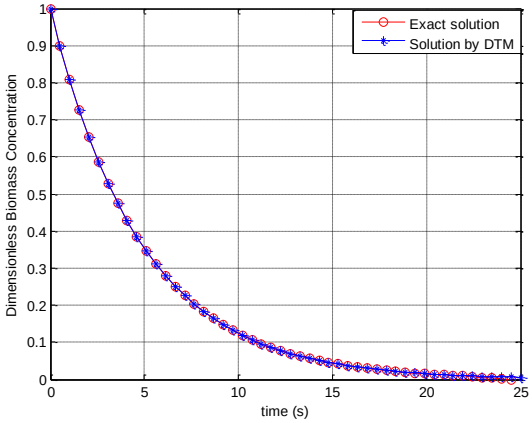


**Figure 13** Comparison of results of biomass concentration against time at isothermal temperature of 1573K

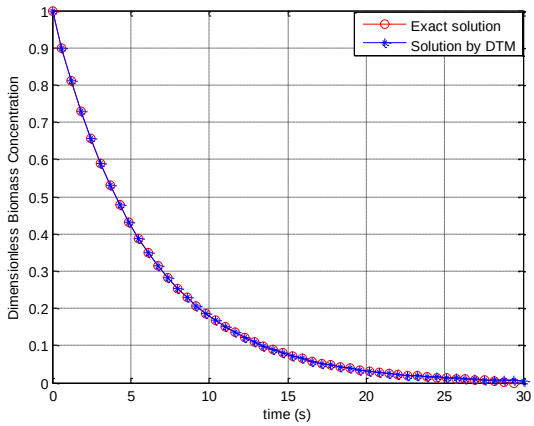


**Figure 14** Comparison of results of biomass concentration against time at an isothermal temperature of 1673K

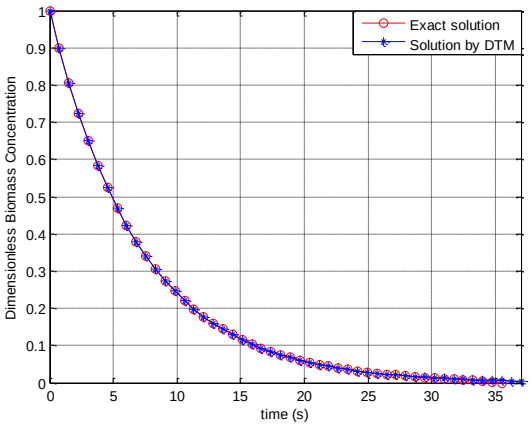


**Figure 15** Comparison of results of biomass concentration against time at isothermal temperature of 1773K

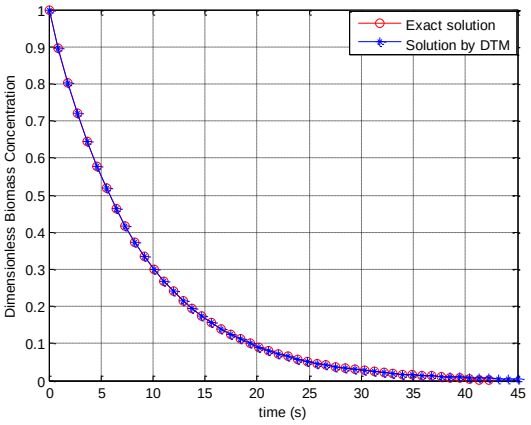


**Figure 16** Comparison of results of Biomass concentration against time at an isothermal temperature of 1873K

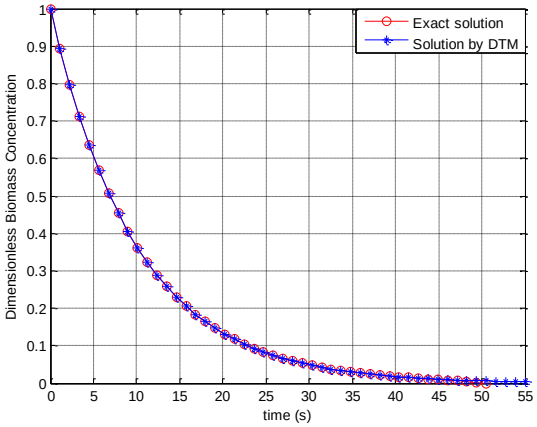


**Figure 17** Comparison of results of biomass concentration against time at isothermal temperature of 1973K

Figs. (18-21) show the effects of isothermal heating temperature (where the pyrolysis temperature maintains a selected constant temperature in a pyrolyzing chamber) on the pyrolysis yield. It should be noted that the results are shown in dimensional forms so as to establish the approximated temperatures at which the various pyrolysis products are formed. From the results, thermal decomposition takes more time at temperature of 473 K and 573 K than that of higher isothermal heating temperature for the biomass particle of the same size. The figures clearly depict that low temperature pyrolysis produces more char and high temperature pyrolysis enhances the production of gas and tar, i.e. an increase in the isothermal heating temperature increases the yield of gaseous products and the decreases char production. The reduced production of tar and gas at low isothermal heating temperature may be due to some resistances to mass or heat transfer inside the particles of the biomass which can be broken by high heating temperature thereby resulting in greater primary decomposition of the sample and higher production of gas and tar at the higher temperature. In each case of the isothermal heating, as the pyrolysis reaches completion, the char production becomes constant.
Also, the results show that the tar rate yield increases first and then decreases and the gas yield increases as the pyrolysis temperature increases, but the char yield significantly decreases as the isothermal temperature increases to 573K and 673K.

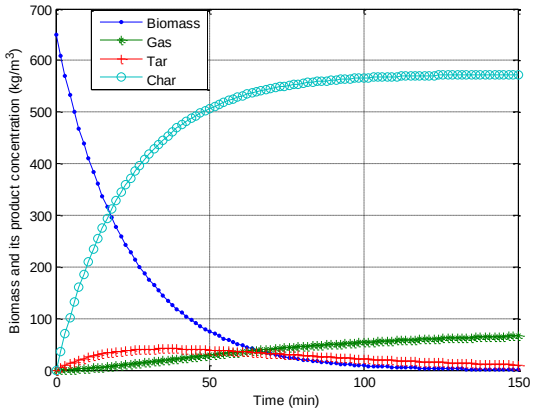


**Figure 18** Biomass concentration against temperature at an isothermal heating temperature of 573K

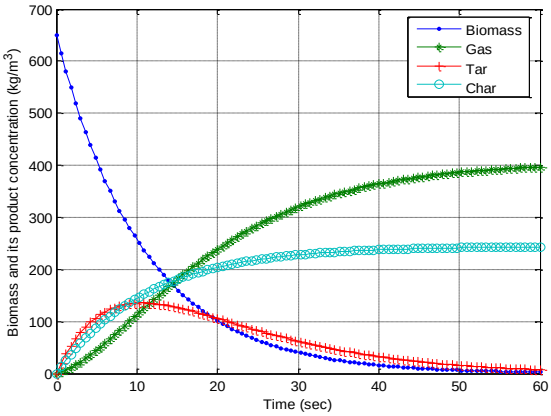


**Figure 19** Production and conversion rate against time at an isothermal heating temperature of 773K

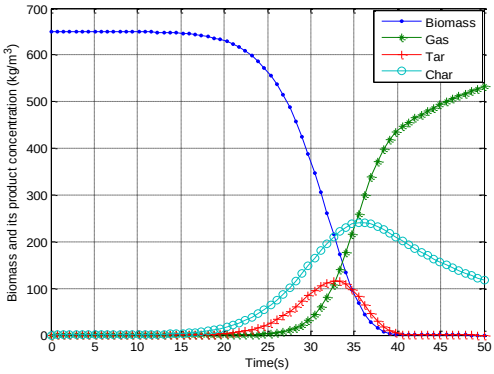


**Figure 20** Biomass and its product concentration variation at heating rate of 10K/s

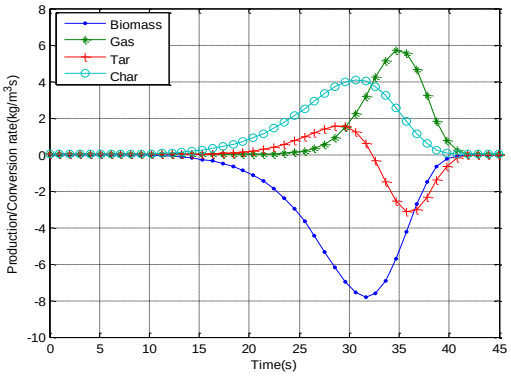


**Figure 21** Production/Conversion rate of Biomass and its Product with time at heating rate of 10K/s

The decrease in the tar yield and sudden increase of gas yield observed at higher temperature may be due to secondary cracking of the pyrolysis liquid in to gaseous product at higher temperature. It could also be deduced from the results that the time required to obtain a certain conversion level decreases with increasing isothermal heating temperature. The trends obtained in this work as shown above are qualitatively the same as reported in literature [24] and [25].

### *4.2 Effects of non-isothermal heating rates on biomass pyrolysis yields*

As pointed out in the previous section, heating rate is one of the important parameter for the yield of different products from the pyrolysis process. To determine the effects of heating rate on the yields of the biomass pyrolysis, simulations were carried out for different heating rates of as shown in Figs. (22-37). The effects of non-isothermal temperature on pyrolysis yields as functions of time are shown in Figs. (22-33) while Figs. (34-37) show the effects of non-isothermal temperature on pyrolysis yields as a function of temperature at an initial particle temperature of 373 K. From the figures, the drying or pre-pyrolysis process are shown as zero rate of production and conversion of the products from 0-120 s and 303-473 K which validates the fact that pyrolysis process actually commenced at about 473K as stated in literatures [25].
It is surprising to see that at any heating rate, the production rate of char is higher than that of tar and gas. This may be due to the increase in the resistance for mass and heat transfers offered by the thick layer of the dried biomass i.e. for the gas and tar to evolve from the particle, they have to travel through a dried layer of the biomass which in consequence, comparably reduces their production rates. Also, it should be noted that increasing the heating rates reduces the particle residence time and as the heating rate are increased, the residence time of volatiles at low or intermediate temperatures decreases. Most of the reactions that favour tar conversion to gas occur at higher temperatures. At low heating rates, the volatiles have sufficient time to escape from the reaction zone before significant cracking can occur.

Also, most of the decomposition takes place at temperatures lower than 500 K, and no more significant decomposition is produced above 750 K. On comparing these results with that of isothermal heating conditions, it is shown that the amount of char produced in the non-isothermal heating conditions is lower than in the isothermal heating conditions.
This is because the isothermal conditions were carried out at relative low temperature and the residual solid contains compounds that evaporate at higher temperatures. The tar yield was low at lower heating rate and slightly increases with increase in heating rate.
The gas yield increases with increase in heating rate while the char yield decreases significantly with increase in heating rate.

The increasing of the tar yield with the increase of heating rate may be due to some resistances to mass or heat transfer inside the particles of the biomass, but increasing the heating rate breaks the heat and mass transfer limitation in the pyrolysis and thereby increasing the tar yield and decreasing char formation.

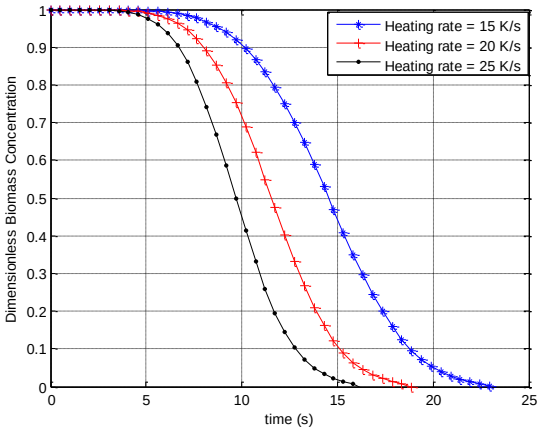


**Figure 22** Biomass concentration against time at non-isothermal condition at an initial temperature of 473K

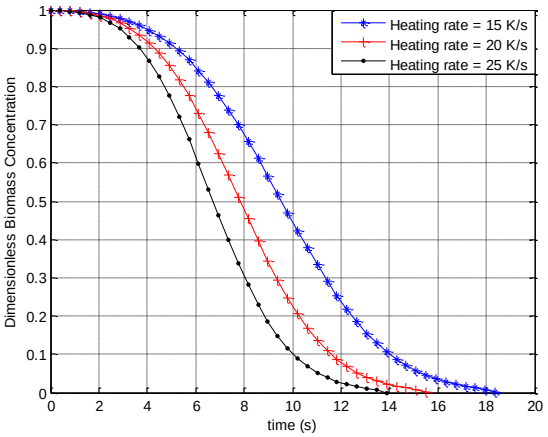


**Figure 23** Biomass concentration against time at non-isothermal condition at an initial temperature of 573K

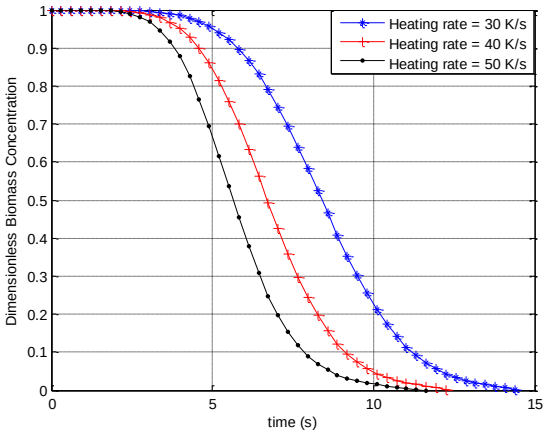


**Figure 24** Biomass concentration against time at non-isothermal condition at an preheating temperature of 473K

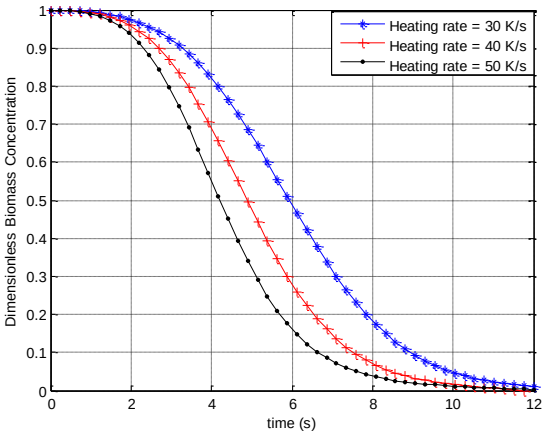


**Figure 25** Biomass concentration against time at non-isothermal condition at an preheating temperature of 573K

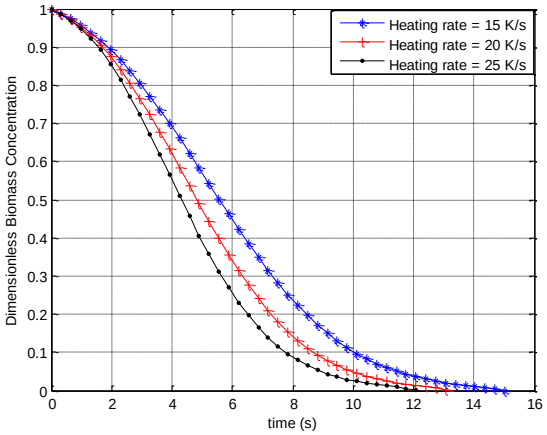


**Figure 26** Biomass concentration against time at non-isothermal condition at an initial temperature of 673K

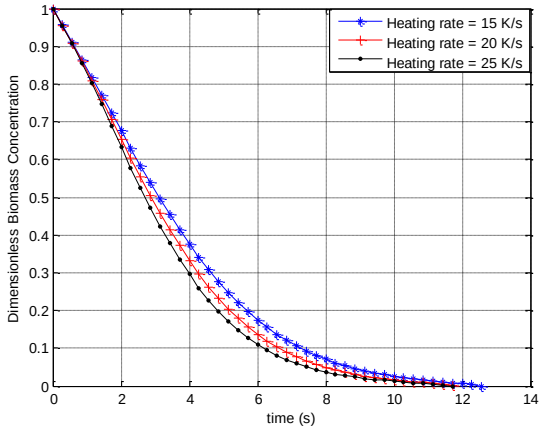


**Figure 27** Biomass concentration against time at non-isothermal condition at an initial temperature of 773K

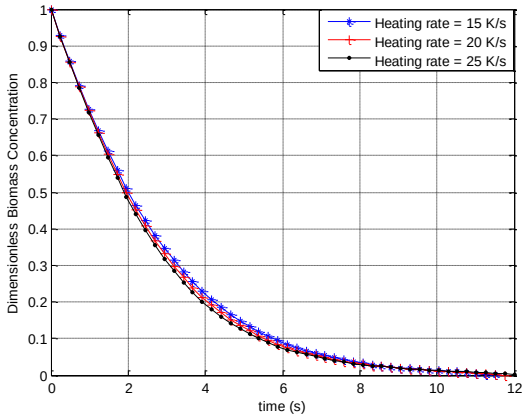


**Figure 28** Biomass concentration against time at non-isothermal condition at an initial temperature of 873K

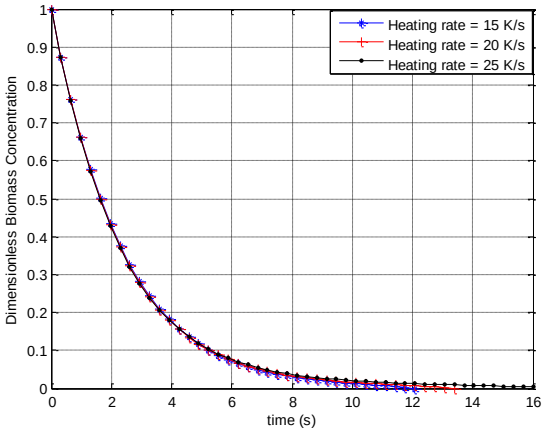


**Figure 29** Biomass concentration against time at non-isothermal condition at an initial temperature of 973K

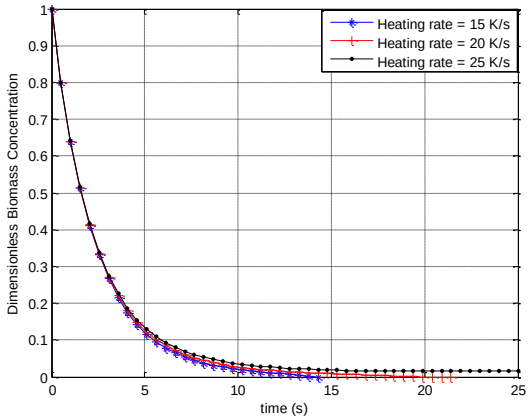


**Figure 30** Biomass concentration against time at non-isothermal condition at an initial temperature of 1073K

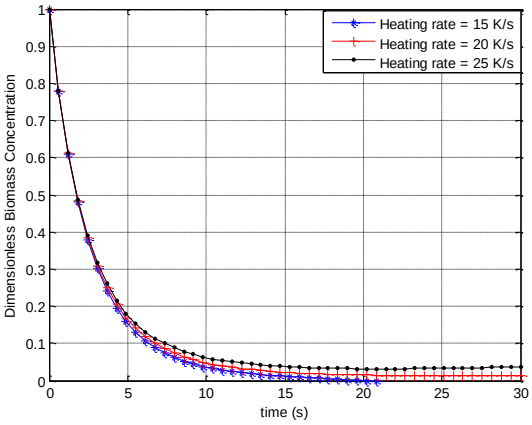


**Figure 31** Biomass concentration against time at non-isothermal condition at an initial temperature of 1173K

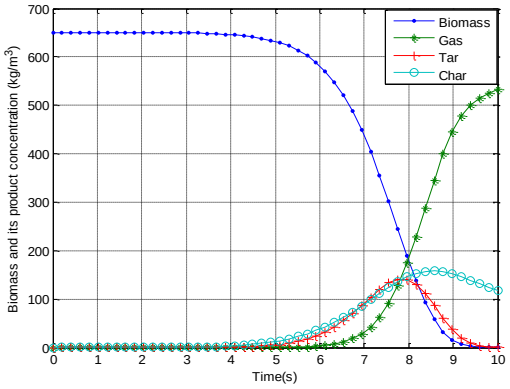


**Figure 32** Biomass and its product concentration variation at heating rate of 50K/s

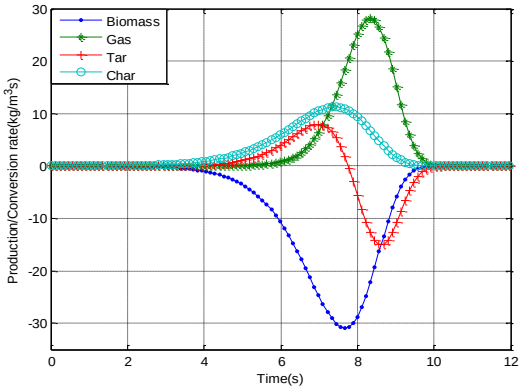


**Figure 33** Production/Conversion rate of Biomass and its Product with time at heating rate of 50K/s

From the Figs (34-37), the rate of char production increases gradually between the particle temperatures of 500 K and 573 K. As the particle temperature increases, gases and tar evolve from the biomass particle and consequently, the rate of char production increases rapidly from

the particle temperature of 500 K to 723 K, after which there is a decrease in the production rate of char (due to the loss of H and O contents of the char at high temperatures) till the whole wood has been pyrolyzed. This shows that pyrolysis process is slowed down from 723-873 K (depending on the heating rates). It could also be inferred from the results that the primary pyrolysis rate of tar production starts gradually from about 573 K till 753 K (depending on the heating rates) and then increases rapidly till the whole tar has been converted to char and gas at the final pyrolysis temperature. The extension of the rate-temperature figure to the negative portion of the graph depicts the conversion rate of tar to char and gas.

### *4.3 Effects of heating rates on particle residence time*

The criteria for characterizing fast pyrolysis based on temperature and heating rate of solid particles that undergoes a thermal decomposition has been advocated by Lédé, and Authier [32]. The effects of heating rates on the particle residence time are shown in Figs. (38-41).
For the low heating rates of 0.01-0.1K/s in Figs. (38), it takes hours or days for the pyrolysis to occur and this will definitely enhance the production of charcoal as depicted in Table (6).

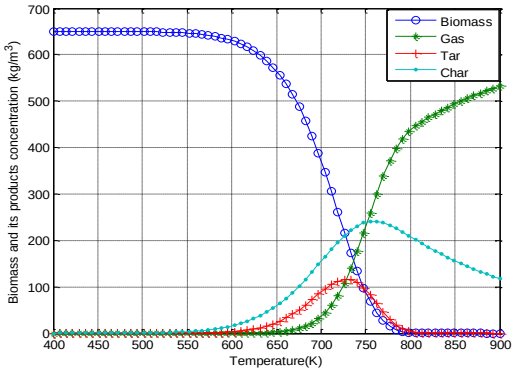


**Figure 34** Biomass and its product concentration variation at heating rate of 10K/s

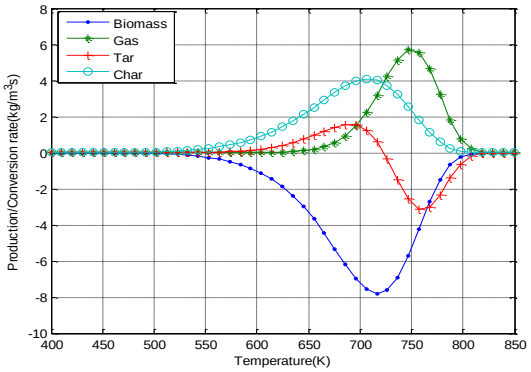


**Figure 35** Production/Conversion rate of Biomass and its Product with temperature at heating rate of 10K/s

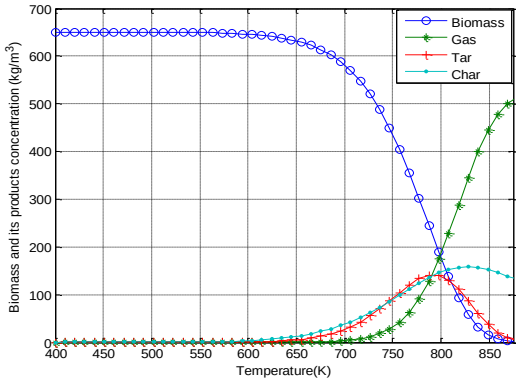


**Figure 36** Biomass and its product concentration variation at heating rate of 50K/

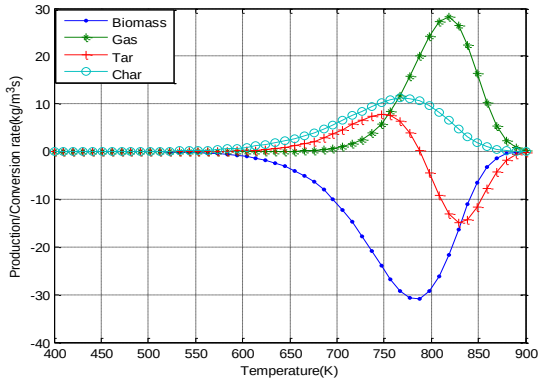


**Figure 37** Production/Conversion rate of Biomass and its Product with temperature at heating rate of 50K/s

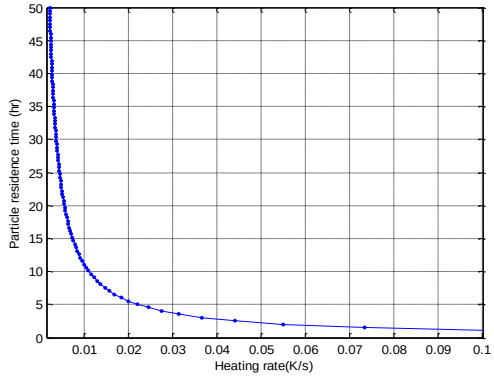


**Figure 38** Variations of biomass particle residence time very low heating rates

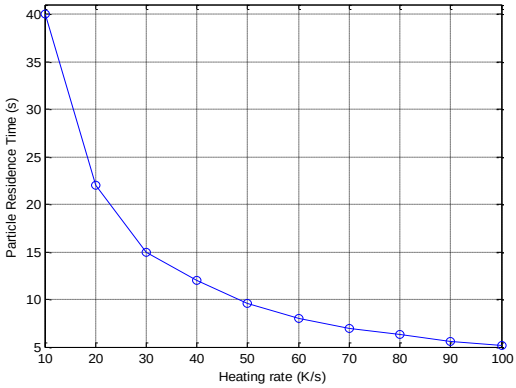


**Figure 39** Variations of biomass particle residence time with heating rates of 10-100K/s

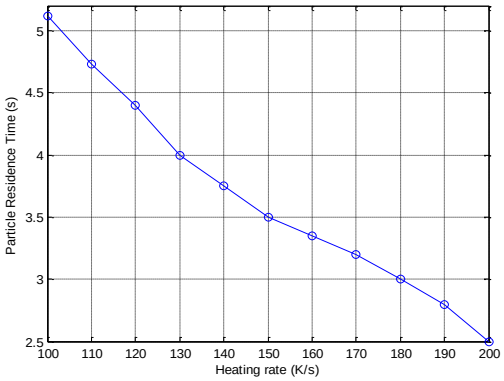


**Figure 40** Variations of biomass particle residence time heating rates of 100-200K,s

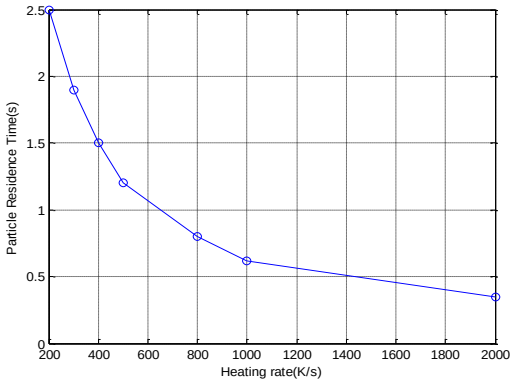


**Figure 41** Variations of biomass particle residence time with heating rates 200-200K/s

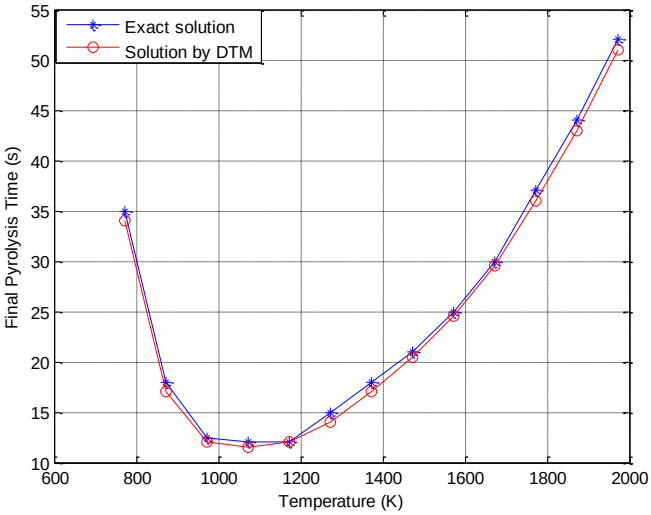


**Figure 42** Effects of heating rates on the particle residence/final pyrolysis time

**Table 6** Pyrolysis conditions for different pyrolysis technologies

| Pyrolysis technology | Residence time | Heating rate | Temperature (°C) | Product |
|---|---|---|---|---|
| Carbonization | days | very low | 400 | charcoal |
| Conventional | 5-30 min | low | 600 | oil, gas, char |
| Fast | 0.5-5s | very high | 650 | bio-oil |
| Flash-liquid | < 1s | high | < 650 | bio-oil |
| Flash-gas | < 1s | high | <650 | chemicals, gas |
| Ultra | < 0.5s | very high | 1000 | chemicals, gas |
| Vacuum | 2-30 s | medium | 400 | bio-oil |
| Hydro-pyrolysis | < 10s | high | < 500 | bio-oil |
| Conventional | < 10s | high | < 700 | chemicals |

The figures show that as the heating rates increases, the particle residence time in the reactor decreases and high heating rates favours the production of tar and gas. Therefore, as shown in the table, the length of heating and its intensity affect the rate and extent of pyrolysis reactions, the sequence of these reactions, and composition of the resultant products. Fig. (38-42) indicated the quantitative values of heating rates and residence time for different pyrolysis products. Such data as these are rarely found in open literatures.

### *4.4 Effects of particle shape, particle size and Biot number on biomass pyrolysis temperature*

Fig. (43) shows the effects of particle shape on the biomass pyrolysis temperature. From the results in Fig. (43), it could be inferred that the spherical particles react most quickly compared to other particles shapes if the characteristics size is taken as the minimum particle dimension. Although the temperature profiles of the three shapes follow the same trend, the pyrolysis process is fastest in spherical particle and slowest in rectangular particle as depicted in the figure. This is because, from the geometrical point of view, the spherical particle has higher surface-area-to-volume ratio which consequently gives it more absorbing capacity than the cylindrical and rectangular particles. Since the sphericity of particle has significant effects on the pyrolysis process, for an effective and efficient performance of biomass gasifier and for optimal yield, a spherical particle should be used.

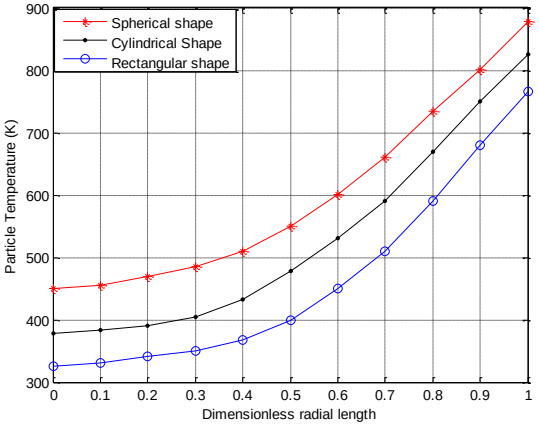


**Figure 43** Effects of particle shape on the biomass pyrolysis temperature

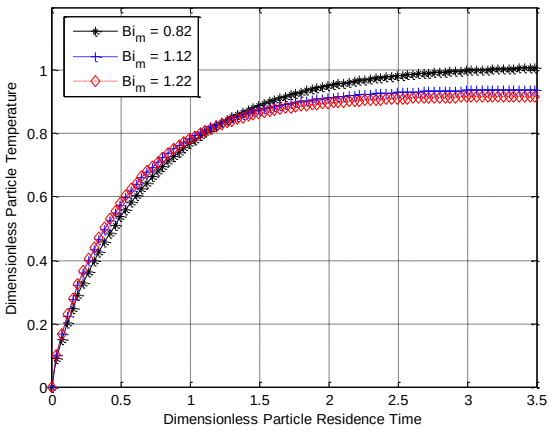


**Figure 44** Effects of Biot number on biomass temperature distributions

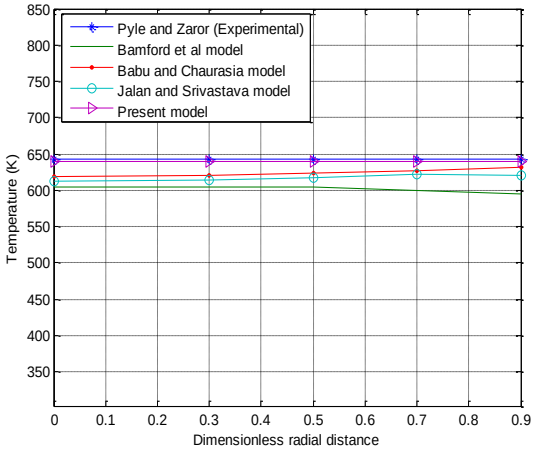


**Figure 45** Comparison of temperature profiles of 11mins pyrolysis process for biomass particle diameter of 0.011m at final pyrolysis temp. of 643K

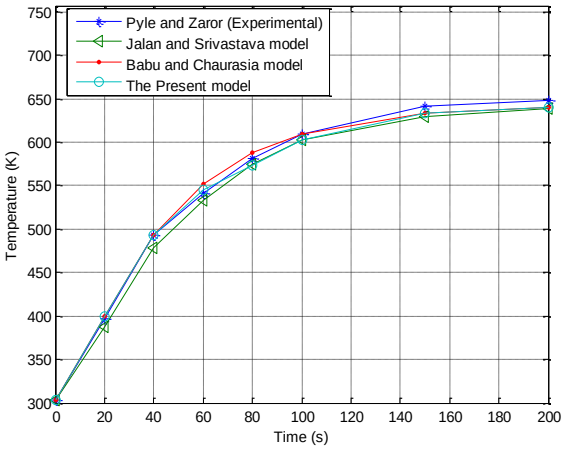


**Figure 46** Comparison of temperature histories for biomass particle diameter of 0.003m at final pyrolysis temp. of 643

Fig. (44) shows the effects of the modified Biot number on the temperature histories. From the results, as the modified Biot number decreases, the temperature history at the center of the thermally thick particle increases. This shows that the temperature history is favoured at values of the modified Biot number less than 1 since more heat is needed to be conducted within the particle to enhance the pyrolysis of the biomass particle than the heat being convected and radiated to the particle surface. Fig. (45) depicts the temperature profiles as predicted with the experimental results and the numerical results of the previous work. From the figure, it could be established that good agreements are obtained between the experimental result and the analytical results predicted in this work.

Also, Fig. (46) shows the comparison of the temperature histories between the experimental results, results of the previous models and the results predicted by the developed closed form solution in this work. The experimental data results were obtained from the work of Pyle and Zaror [1], and the previous theoretical results obtained through numerical solutions by Jalan and Srivastava [21] and Babu and Chaurasia [23] at the centre of the cylindrical pellet.
It could be seen from the Fig. (44) that as the Biot number decreases, the model becomes an increasingly good predictor. The model is adequate at $Bi_m$ less than 1 which shows almost indistinguishable results from the experimental results of Pyle and Zaror. The region of the validity of the model is defined by the value of Biot number that is less than 1. It was found that the models developed in the present study are in excellent agreement with the experimental data and in the region of validity it presents better results in agreement with the experimental results than the other developed model as it shown in Table (5).
Fig. (47) shows the temperature history of the particle at different locations in the particle of half thickness 0.01 m when there is convective and radiative heat transfer at the surface of the particle. From the figure, it shows that it takes about 700 Sec for the pyrolysis final temperature to be reached.
Fig. (48) shows the temperature profile of the particle at different time interval when there is convective and radiative heat transfer at the surface of the particle of half thickness 0.01 m. From the figure, it shows that the higher the particle residence time in the reactor, the higher the particle temperature.
Fig. (49) shows the temperature history of the particle of half thickness 0.003 m when constant temperature is applied to the surface of the slab/chip.

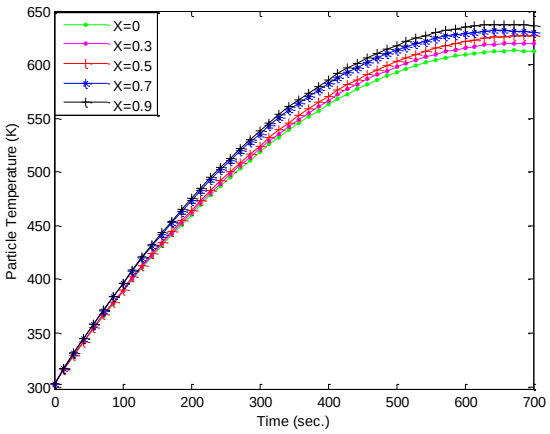


**Figure 47** Temperature history of the particle at To=303K, half thickness=0.011m, $T_f$=643K

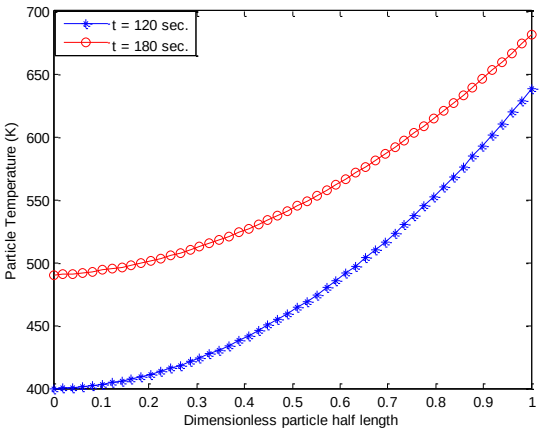


**Figure 48** Temperature profile of the particle at To=303K, half thickness=0.011m, $T_f$=753K

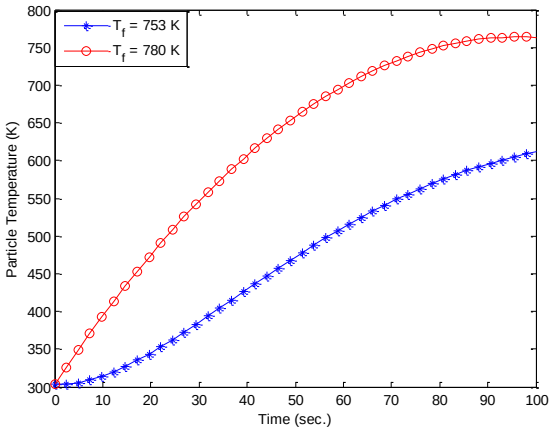


**Figure 49** Temperature history of the particle at To=303K, half thickness=0.003m, Tf=643K

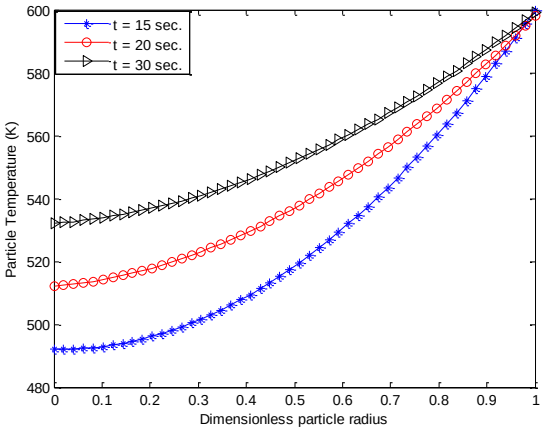


**Figure 50** Temperature profile of the particle at To=473K, radius=0.005 m, $T_{\text{constant wall temp.}}$=600 K

From the figure, it is observed that as the constant wall temperature increased, the pyrolysis final time decreased i.e. the pyrolysis time is completed faster. Fig. (50) shows the temperature profiles at various time intervals of the particle of half thickness 0.005 m when constant temperature of 600 K is applied to the surface of the slab/chip. From the figure, it shows that the longer the pyrolysis time applied to the surface of the particle, the higher the pyrolysis temperature.

## 7 Conclusion

In this work, differential transformation method has been used to develop analytical solutions of integrated kinetic and heat transfer models of pyrolysis of biomass particles. The results from the analytical models were shown to be in good agreements with the reported experimental and numerical results in literature. The analytical models were used to investigate the effects of heating conditions, heat of reaction, convective and radiative heat transfer, particle sizes and shapes and boundary conditions on the pyrolysis of a biomass particle. The work has a lot of practical importance and physical significance in industrial pyrolysis applications and in the design of biomass gasifiers, reactors etc.

Also, the findings of the work show that simple kinetic and heat transfer models of the pyrolysis are generally adequate especially in the slow pyrolysis of biomass particle.

## References

[1] Pyle, D. L., and Zaror, C. A., "Heat Transfer and Kinetics in the Low Temperature Pyrolysis of Solids", Chemical Engineering Science, Vol. 39, pp. 147–158, (1984).

[2] Bamford, C. H., Crank, J., and Malan, D. H., "The Combustion of Wood Part I", Proceedings of the Cambridge Philosophical Society, Vol. 42, pp. 166–182, (1946).

[3] Roberts, A. F., and Clough, G., "Thermal Degradation of Wood in an Inert Atmosphere", In: Proceedings of the Ninth Symposium (International) on Combustion, the Combustion Institute, Pittsburgh, pp. 158–167, (1963).

[4] Weatherford, W. D., and Sheppard, D. M., "10th int. Symposium on Combustion", the Combustion Institute, Pitts, pp. 897, (1965).

[5] Tinney, E. R., "The Combustion of Wood Dowels in Heated Air", In: Proceedings of the 10th Symposium (International) on Combustion, The Combustion Institute, Pittsburgh, pp. 925–930, (1965).

[6] Matsumoto, T., Fujiwara T., and Kondo, J., "12th int. Symposium on Combustion, the Combustion Institute, Pitts, pp. 515, (1969).

[7] Roberts, A. F., "13th Int. Symposium on Combustion, the Combustion Institute, Pitts, pp. 893, (1971).

[8] Kung, H. C., "A Mathematical Model of Wood Pyrolysis", Combustion and Flame, Vol. 18, pp. 185–195, (1972),

[9] Maa, P. S., and Bailie, R. C., "Combustion Science and Technology", Vol. 7, pp. 257, (1973).

[10] Kansa, E. J., Perlee H. E., and Chaiken, R., "Mathematical Model of Wood Pyrolysis Including Internal Forced Convection, Combustion and Flame, Vol. 29, pp. 311–324, (1977),

[11] Chan, W. R., Kelbon, M., and Krieger, B. B., "Modeling and Experimental Verification of Physical and Chemical Processes during Pyrolysis of Large Biomass Particle", Fuel 64, pp. 1505–1513, (1985),

[12] Koufopanos, C. A., Papayannakos, N., Maschio, G., and Lucchesi, A., "Modelling of the Pyrolysis of Biomass Particles, Studies on Kinetics, Thermal and Heat Transfer e4ects, the Canadian Journal of Chemical Engineering, Vol. 69, pp. 907–915, (1991),

[13] Lee, C. K., Chaiken, R. F., and Singer, J. M., "Charring Pyrolysis of Wood in 0res by Laser Simulation", In: Proceedings of the 16th Symposium (International) on Combustion, the Combustion Institute, Pittsburgh, pp. 1459–1470, (1976).

[14] Miyanami, K., Fan, L. S., Fan L. T., and Walawender, W. P., "A Mathematical Model for Pyrolysis of a Solid Particle Effects of the Heat of Reaction", the Canadian Journal of Chemical Engineering, Vol. 55, pp. 317–325, (1977).

[15] Fan, L. T., Fan, L. S., Miyanami, K., Chen, T. Y., and Walawender. W. P., "A mathematical Model for Pyrolysis of a Solid Particle Effects of the Lewis Number", the Canadian Journal of Chemical Engineering, Vol. 55, pp. 47–53, (1977).

[16] Simmons, G. M., and Gentry, M., "Particle Size Limitations Due to Heat Transfer in Determining Pyrolysis Kinetics of Biomass", J. Anal. and Appl. Pyrolysis, Vol. 10, pp. 117-127, (1986).

[17] Villermaux, J., Antoine, B., Lede, J., and Soulignac, F., "A New Model for Thermal Volatilization of Solid Particles undergoing Fast Pyrolysis", Chemical Engineering Science, Vol. 41, pp. 151–157, (1986).

[18] Di Blasi, C., "Analysis of Convection and Secondary Reaction Effects within Porous Solid Fuels undergoing Pyrolysis", Combustion Science and Technology, Vol. 90, pp. 315–340. (1993).

[19] Melaaen, M. C., and Gronli, M. G., "Modeling and Simulation of Moist Wood Drying and Pyrolysis", In: Bridgwater, A.V., Boocock, D.B.G. (Eds.), Developments in Thermochemical Biomass Conversion, Blackie, London, pp. 132–146, (1997).

[20] Jalan, R. K., and Srivastava, V. K., "Studies on Pyrolysis of a Single Biomass Cylindrical Pellet–kinetic and Heat Transfer Effects", Energy Conversion and Management, Vol. 40, pp. 467–494, (1999).

[21] Ravi, M. R., Jhalani, A., Sinha, S., and Ray, A., "Development of a Semi-empirical Model for Pyrolysis of an Annular Sawdust Bed", Journal of Analytical and Applied Pyrolysis, Vol. 71, pp. 353-374, (2004).

[22] Babu, B. V., and Chaurasia, A. S., "Modeling for Pyrolysis of Solid Particle: Kinetics and Heat Transfer Effects", Energy Conversion and Management, Vol. 44, pp. 2251–2275, (2003),

[23] Sheth, P. N., and Babu, B. V., "Kinetic Modeling of the Pyrolysis of Biomass National Conference on Environmental Conservation, Pilani, India, pp. 453-458, (2006).

[24] Yang, Y. B., Phan, A. N., Ryu, C., Sharifi, V., and Swithenbank, J., "Mathematical Modelling of Slow Pyrolysis of Segregated Solid Wastes in a Packed-bed Pyrolyser Elsevier Journal of Fuel, (2006).

[25] Mandl, C., Obernberger, I., and Biedermann, F., "Updraft fixed-bed Gasification of Softwood Pellets: Mathematical Modelling and Comparison with Experimental Data In: Proceedings of the 17, European Biomass Conference & Exhibition Hamburg, Italy, (2009).

[26] Weerachanchai, P., Tangsathitkulchai, C., and Tangsathitkulchai, M., "Comparison of Pyrolysis Kinetic Model for Thermogravimetric Analysis of Biomass", Suranree Journal of Tecnologies, Vol. 17, No. 4, pp. 387-400, (2010).

[27] Slopiecka, K., Bartocci, P., and Fantozzi, F., "Thermogravimetric Analysis and Kinetic Study of Poplar Wood Pyrolysis", 3rd International Conference on Applied Energy, Perugia, Italy, pp. 1687-1698, (2011).

[28] Gauthier, G., Melkior, T., Salvador, S., Corbetta, M., Frassoldati, A., Pierucci, S., Ranzi, E., Bennadji, H., and Fisher, E.M., "Pyrolysis of Thick Biomass Particles: Experimental and Kinetic Modelling", Chemical Engineering Transactions, Vol. 32, (2013).

[29] Suriapparao, D. V., and Vinu, R., "Effects of Biomass Particle Size on Slow Pyrolysis Kinetics and Fast Pyrolysis Product Distribution", Waste Biomass Valorization, (2017).

[30] Bennadji, H., "Low-Temperature Pyrolysis of Woody Biomass in the Thermally Thick Regime", Energy & Fuels, Vol. 27, No. 3, pp. 1453-1459, (2013).

[31] Ranzi, E., "Comprehensive and Detailed Kinetic Model of a Traveling Grate Combustor of Biomass", Energy and Fuels, Vol. 25, No. 9, pp. 4195-4205, (2011).

[32] Park, W.C., Atreya, A., and Baum, H.R., "Experimental and Theoretical Investigation of Heat and Mass Transfer Processes during Wood Pyrolysis", Combustion and Flame, Vol. 157, No. 3, pp. 481-494, (2010).

[33] Norinaga, K., et al. "Detailed Chemical Kinetic Modelling of Vapour-phase Cracking of Multi-component Molecular Mixtures Derived from the Fast Pyrolysis of Cellulose", Fuel, Vol. 103, pp. 141-150, (2013).

[34] Ranzi, E., "Hierarchical and Comparative Kinetic Modeling of Laminar Flame Speeds of Hydrocarbon and Oxygenated Fuels", Progress in Energy and Combustion Science, Vol. 38, No. 4, pp. 568-501, (2012).

[35] Gentile, G., Eduardo, P., Debiagi, A., Cuoci, A., Frassoldati, E., Ranzi, T., and Faravelli, A., "Computational Framework for the Pyrolysis of Anisotropic Biomass Particles", Chemical Engineering Journal, Article in Press, (2017).

[36] Anca-Couce, A., "Reaction Mechanisms and Multi-scale Modelling of Lignocellulosic Biomass Pyrolysis", Progress in Energy and Combustion Science, Vol. 53, pp. 41-79, (2016).

[37] Mettler, M.S., Vlachos, D.G., and Dauenhauer, P.J., "Top Ten Fundamental Challenges of Biomass Pyrolysis for Biofuels", Energy & Environmental Science 5, pp. 7797-7809, (2012).

[38] Cuoci, A., Frassoldati, T., Faravelli, E., and Ranzi, A., "Computational Tool for the Detailed Kinetic Modeling of Laminar Flames: Application to C2H4/CH4 Coflow Flames", Combustion and Flame, Vol. 160, pp. 870-886, (2013).

[39] Cuoci, A., Frassoldati, T., Faravelli, E., and Ranzi, "Open SMOKE++: An Object-oriented Framework for the Numerical Modeling of Reactive Systems with Detailed Kinetic Mechanisms", Computer Physics Communications, Vol. 192, pp. 237-264, (2015).

[40] Maffei, T., Gentile, G., Rebughini, S., Bracconi, M., Manelli, F., Lipp, S., Cuoci, A., and Maestri, M., "A Multiregion Operator-splitting CFD Approach for Coupling Microkinetic Modeling with Internal Porous Transport in Heterogeneous Catalytic Reactors", Chemical Engineering Journal, Vol. 283, pp. 1392-1404, (2016).

[41] Blondeau, J., and Jeanmart, H., "Biomass Pyrolysis at High Temperatures: Prediction of Gaseous Species Yields from an Anisotropic Particle", Biomass and Bioenergy, Vol. 41, pp. 107-121, (2012).

[42] Gronli, M., "A Theoretical and Experimental Study of the Thermal Conversion of Biomass", PhD Thesis, NTNU, Trondheim, (1996).

[43] Bennadji, H., Smith, K., Shabangu, S., and Fisher, E.M., "Low-temperature Pyrolysis of Woody Biomass in the Thermally Thick Regime, Energy & Fuels, Vol. 27, pp. 1453-1459, (2013).

[44] Corbetta, M., Frassoldati, A., Bennadji, H., Smith, K., Serapiglia, M.J., Gauthier, G., Melkior, T., Ranzi, E., and Fisher, E.M., "Pyrolysis of Centimeter-scale Woody Biomass Particles: Kinetic Modeling and Experimental Validation, Energy & Fuels, Vol. 28, pp. 3884-3898, (2014).

[45] Gauthier, G., "Syntesis of Second Generation Biofuels: Study of Pyrolysis of Centimeter-scale Wood Particles at High Temperature", Univerisite de Toulouse, (2013).

[46] Gauthier, G., Melkior, T., Grateau, M., Thiery, S., and Salvador, S., "Pyrolysis of Centimetre-scale Wood Particles: New Experimental Developments and Results", Journal of Analytical and Applied Pyrolysis, Vol. 104, pp. 521-530, (2013).

[47] Paulsen, A.D., Hough, B.R., Williams, C.L., Teixeira, A.R., Schwartz, D.T., Pfaendtner, J., and Dauenhauer, P.J., "Fast Pyrolysis of Wood for Biofuels: Spatiotemporally Resolved Diffuse Reflectance in Situ Spectroscopy of Particles", ChemSusChem, Vol. 7, pp. 765-776, (2014).

[48] Ranzi, E., Cuoci, A., Faravelli, T., Frassoldati, A., Migliavacca, G., Pierucci, S., and Sommariva, S., "Chemical Kinetics of Biomass Pyrolysis", Energy & Fuels, Vol. 22, pp. 4292-4300, (2008).

[49] Debiagi, P.E.A., Pecchi, C., Gentile, G., Frassoldati, A., Cuoci, A., Faravelli, T., and Ranzi, E., "Extractives Extend the Applicability of Multistep Kinetic Scheme of Biomass Pyrolysis", Energy & Fuels, Vol. 29, pp. 6544-6555, (2015).

[50] Debiagi, P.E.A., Gentile, G., Pelucchi, M., Frassoldati, A., Cuoci, A., Faravelli, T., and Ranzi, E., "Detailed Kinetic Mechanism of Gas-phase Reactions of Volatiles Released from Biomass Pyrolysis", Biomass and Bioenergy, Vol. 93, pp. 60-71, (2016).

[51] Zaror, C. A., "Studies of the Pyrolysis of Wood at Low Temperatures", PhD. Dissertation, University of London", (1982).

[52] Ojolo, S. J., Osheku, C. A., and Sobamow, M. G., "Analytical Investigations of Kinetic and Heat Transfer in Slow Pyrolysis of a Biomass Particle", Int. Journal of Renewable Energy Development, Vol. 2, No. 2, pp. 105-115, (2013).

[53] Sobamowo, M.G., Ojolo, S. J., Osheku, C. A., and Kehinde, A. J., "Heat Transfer Analysis in Pyrolysis of Different Shapes Biomass Particles Subjected to Different Boundary Conditions", Integral Transform Methods, Journal of Heat and Mass Transfer Research, Article in Press.

[54] Bidabadi, M., Mostafavi, S. A., Dizaji, F. F., and Dizaji. B. H., "An Analytical Model for Flame Propagation through Moist Lycopodium Particles with Non-unity Lewis Number [J]. International Journal of Engineering, Vol. 27, No. 5, pp. 793−802, (2014).

[55] Dizaji, B. H., and Bidabadi, M., "Analytical Study about the Kinetics of Different Processes in Pyrolysis of Lycopodium Dust [J]. Journal of Fuel and Combustion, Vol. 6, No. 2, pp. 13−20, (2014), (in Persian)

[56] Lédé, J., and Authier, O., "Temperature and Heating rate of Solid Particles undergoing a Thermal Decomposition", which Criteria for Characterizing Fast Pyrolysis Journal of Analytical and Applied Pyrolysis, Vol. 113, pp. 1-14, (2015).

[57] Font, R., Marcilla, A., Verdu, E., and Devesa, J., "Kinetics of the Pyrolysis of Almond Shells and Almond Shells Impregnated with $COCl_2$ in a Fluidized Bed Reactor and in a Pyroprobe 100, Industrial and Engineering Chemistry Research, Vol. 29, pp. 1846–1855, (1990).

[58] Shafizadeh, F., and Chin, P.P.S., "Thermal Deterioration of Wood", ACS Symposium Series Vol. 43, pp. 57–81, (1977).

[59] Thurner, F., and Mann, U., "Kinetic Investigation of Wood Pyrolysis", Industrial and Engineering Chemical Process Design and Development, Vol. 20, pp. 482–488, (1981).

[60] Janse, A.M.C., Westerhout, A.M.C., and Prins, W., "Modelling of Flash Pyrolysis of a Single Wood Particle", Chemical Engineering and Processing, Vol. 39, pp. 239-252, (2000).

[61] Srivastava, V. K., Sushil and Jalan, R. K., "Prediction of Concentration in the Pyrolysis of Biomass Materials-II", Energy Conversion and Management, Vol. 37, No. 4, pp. 473-483, (1996).

[62] Liden, C. K., Berruti, F., and Scott, D. S., "A Kinetic Model for the Production of Liquids from the Flash Pyrolysis of Biomass", Chem. Eng. Commun, Vol. 65, pp. 207–221, (1988).

[63] Prakash, N., and Karunanithi, T., "Kinetic Modelling in Biomass Pyrolysis a Review", Journal of Applied Sciences Research, Vol. 4, No. 12, pp. 1627-1636, (2008),

[64] Branca, C., and Di Blasi, C., "Kinetics of the Isothermal Degradation of Wood in the Temperature Range, 528-708 K. Journal of Analytical and Applied Pyrolysis, Vol. 67, pp. 207-219, (2003),

[65] Holman, J. P., "*Heat Transfer*", Sixth Edition, McGraw-Hill Book Company, (1986).

[66] Zhou, J.K., "Differential Transformation and its Applications for Electrical Circuits", Huazhong University Press, Wuhan, China, (1986). (in Chinese).

[67] Sobamowo, M. G., "Nonlinear Analysis of Flow-induced Vibration in Fluid-conveying Structures using Differential Transformation Method with Cosine-after Treatment Technique", Transaction of Iranian Society of Mechanical Engineers, Vol. 18, No. 1, pp. 43-63, Publication of Iranian Society of Mechanical Engineers, (2018),

[68] Sobamowo, M. G., Jayesimi, L. O., and Waheed, M. A., "Axisymmetric Magneto hydrodynamic Squeezing Flow of Nanofluid in a Porous Medium under the Influence of Slip Boundary Conditions Transport Phenomena in Nano and Micro Scales", Vol. 6, No. 2, pp. 122-132, Publication of University of Sistan and Baluchestan, Iranian Society of Mechanical Engineers, Iran, (2018),

[69] Sobamowo, M. G., "Nonlinear Thermal and Flow-induced Vibration Analysis of Fluid-Conveying Carbon Nanotube Resting on Winkler and Pasternak Foundations", Thermal Science and Engineering Progress, Elsevier, Vol. 4, pp. 113-149, (2017).

[70] Sobamowo, M. G., "Singular Perturbation and Differential Transform Methods to Two-dimensional Flow of Nanofluid in a Porous Channel with Expanding/contracting Walls Subjected to a Uniform Tranverse Magnetic Field", Thermal Science and Engineering Progress, Vol. 4, pp. 71-84, Elsevier, (2017),

[71] Sobamowo, M. G., Ojolo, S. J., and Osheku, C. A., "Analysis of Pyrolysis Kinetics of Biomass Particle under Isothermal and Non-isothermal Heating Conditions using Differential Transformation Method", Global Journal of Research in Engineering, Vol. 17, No. 6, pp. 1-21, Global Journal Inc. USA, (2017).

[72] Sobamowo, M. G., Jayesimi, L. O., and Waheed, M. A., "On the Squeezing Flow of Nanofluid through a Porous Medium with Slip Boundary and Magnetic Field: A Comparative Study of Three Approximate Analytical Methods", Global Journal In. USA, Vol. 17, No. 6, pp. 61-67, (2017).

[73] Adeleye, O. A., Olawale, O. L., and Sobamowo, M. G., "Prediction of Phagocyte Transmission for Foreign Body Responses to Subcutaneous Biomaterial Implantations using Differential Transform Method", Journal of Biomimetrics, Biomaterials and Biomedical Engineering, Vol. 32, pp. 98-114, Trans Tech Publications, Switzerland, (2017).

[74] Holman, J. P., "*Heat Transfer*", Sixth Edition, McGraw-Hill Book Company, (1986).

## Nomenclature

$A_1; A_2; A_3; A_4; A_5$ frequency factor, 1/s
$Bi_m$ Modified Biot number
C concentration, kg/m$^3$
$C_p$ specific heat capacity, J/kgK
E activation energy, J/mol
h convective heat transfer coefficient, W/m$^2$ K
K thermal conductivity, W/mK
$k_1; k_2; k_3; k_4; k_5$ rate constants, 1/s
Q heat of pyrolysis, J/Kg

r radial distance, m
R radius for cylindrical particle, m
$R_g$ universal gas constant, J/mol
t time, s
$T_f$ reactor final temperature, K
T temperature, K
R' dimensionless radial distance

*Greek letters*
ρ Bulk density of wood, $Kg/m^3$
$\rho_\infty$ Ultimate density of wood, $Kg/m^3$
τ dimensionless time
θ dimensionless temperature
ϵ emissivity coefficient
ε void fraction of particle
σ Stefan Boltzmann constant, $W/m^2 K^4$
α Heat of reaction number

*Subscripts*
B virgin biomass
G gases
C char
T tar
G gas
0 initial
f final

## چکیده

رفتار غیر خطی ذاتی در مدلهای سینتیک و انتقال حرارت در طی پیرولیز (تجزیه حرارتی) زیست توده‌ها منجر به توسعه روشهای عددی در مسائل غیرخطی شده است. به هر حال، به منظور فهم فیزیکی موضوع و نشان دادن ارتباط مستقیم بین پارامترهای مدل، راه حلهای تحلیلی مورد نیاز است.
در این تحقیق به کمک حل تبدیل دیفرانسیلی، پاسخ تحلیلی تقریبی برای سینیتیک و انتقال حرارت یک‌پارچه ذرات در طی پیرولیز زیست توده در شرایط گرمایش هم‌دما و غیر هم‌دما ارائه شده است. همچنین، نتایج حل تحلیلی با نتایج حل عددی موجود در سوابق علمی مقایسه شده است. از این رو، مطالعات پارامتری برای بررسی اثرات حرارتی، نرخ حرارت، پارامترهای ترمو-هندسی، شرایط مرزی، شکل ذرات و اندازه بر روی پیرولیز سینتیک و حرارتی در طی تجزیه ذرات زیست توده صورت پذیرفته است. لذا، انتظار می‌رود که این مطالعه فهم فیزیکی عوامل و فاکتورهای مختلف موثر بر این پدیده ترموشیمیایی را فراهم کند.